INTERNATIONAL ATOMIC ENERGY AGENCY
UNITED NATIONS EDUCATIONAL, SCIENTIFIC AND CULTURAL ORGANIZATION

INTERNATIONAL CENTRE FOR THEORETICAL PHYSICS
34100 TRIESTE (ITALY) - P.O.B. 586 - MIRAMARE - STRADA COSTIERA 11 - TELEPHONE: 9240-1
CABLE: CENTRATOM - TELEX 460892 - 1

SMR/291 - 43

SPRING COLLEGE IN CONDENSED MATTER
ON
"THE INTERACTION OF ATOMS & MOLECULES WITH SOLID SURFACES"
(25 April - 17 June 1988)

MOLECULE-SURFACE SCATTERING

Andrew E. DEPRISTO
Department of Chemistry
Iowa State University
Ames, IA 50011
U.S.A.

MOLECULE-SURFACE SCATTERING: I

In these lectures, I will introduce the concepts and methods associated with the scattering of molecules from clean, perfectly periodic solid surfaces. I will not discuss scattering from adsorbate covered and/or non-periodic surfaces since these areas are much more complex computationally and/or insufficiently advanced conceptually. Even with this restriction, such a wide variety of physical phenomena can occur in the scattering that it will not be possible to describe these in only five lectures. Let me first just mention the types of phenomena, and then I will indicate the restricted range that I will consider.

A "cartoon" illustration of the various scattering processes is shown in Figure 1.1. In the simplest scattering event, a molecule reflects elastically from the solid, changing the direction of its momentum in the process called diffraction. A slightly more complex situation occurs when the molecule also changes its internal rotational, vibrational and/or electronic states, a process termed inelastic scattering. Even more complexity occurs if the molecular identity can change such as in the dissociative chemisorption event, $AB(g) + M \rightarrow A(a) + B(a) + M$. (Throughout this article, I refer to solid surfaces by the symbol "M", a gas phase species by "(g)" and an adsorbed species by "(a)"). Finally, it is also possible to have the scattering event disrupt the surface by ejecting surface atoms into the gas phase either directly by sputtering or indirectly by forming volatile molecular species via reaction between the gas molecule and the surface atoms. In all of these processes, transfer of energy between the molecular and solid degrees of freedom may occur. The relevant solid's degrees of freedom for low energy excitations involve

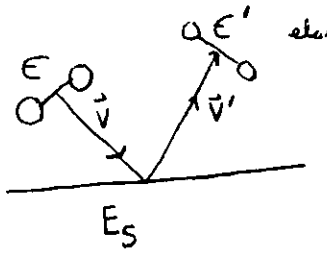

elastic : $|\vec{v}'| = |\vec{v}|$
$\epsilon' = \epsilon$
$E_s' = E_s$

inelastic : $|\vec{v}'| \neq |\vec{v}|$
$\epsilon' \neq \epsilon$
$E_s' \neq E_s$

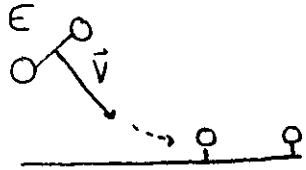

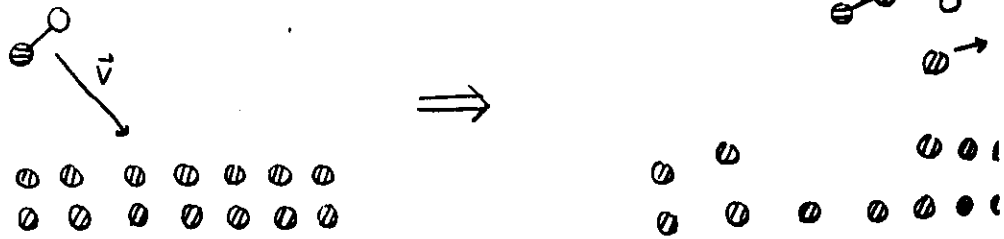

Figure 1.1

motion of the nuclei (i.e. phonons), and for metals excitation and deexcitation of electrons with energies close to the Fermi level (i.e. electron-hole pair or (e,h) processes). High energy excitations include collective excitation of the free electrons in a metal (i.e. plasmons), electronic excitation of core electrons of the surface atom, and the previously mentioned ejection of the surface atoms.

From the above list, I will consider only elastic, inelastic and dissociative chemisorption events. For these cases, I will also describe the treatment of low energy excitation modes in the solid. The major emphasis will be on dissociative chemisorption since this is among the simplest reactive scattering event occurring on surfaces. It is also a relatively new area to attract considerable theoretical attention. By contrast, elastic and inelastic scattering have been subjected to intensive theoretical studies by many workers for over a decade, and for certain simple problems, much longer. A large literature is available for such processes [1-5 and references therein], including a well-written (though slightly outdated) book, "Dynamics of Gas-Surface Scattering."[1] A number of reviews have appeared over the last decade [2-5]. A recent comprehensive review of theory [4] by Gerber provides an introduction to a number of topics, along with a representative reference list. I highly recommend this article.

High energy scattering in which the surface atoms are ejected has been treated by a number of research groups. The interested reader is referred to the work of Garrison and co-workers for an introduction and relevant references [6]. To my knowledge, theoretical treatments of the dynamics of formation of volatile products such as in the reaction of F with Si to form

SiF_n are not sufficiently advanced to warrant a description since the underlying potential energy surface (PES) is essentially unknown, and must be extremely complex to describe the many arrangements occurring in such processes. There is little experience with multi-arrangement PES in simpler gas phase systems not to mention in extended systems. I will also not describe dissociation of gas phase species via such processes as AB(g) + M -> A(g) +B(g) + M or AB(g) + M -> A(a) + B(g) + M. This area is more complex than dissociative chemisorption since one or two more arrangements must be included in a PES. These are generally higher energy channels since at most only one gas-surface bond is formed to compensate for the breaking of the molecular bond. At present, these have been treated using only the simplest PES not allowing for multiple rearrangement channels. The reader is referred to the work of Gerber and coworkers as reviewed in reference 4 for more details.

The reason I have restricted consideration to the above mentioned processes has to do with the kinetic energy of the incident molecule. Thermally activated chemical processes are typically limited to temperatures below 2000K, about .18 eV. Even assuming that the molecules in the high energy tail of a Boltzmann velocity distribution are important, it is rather unlikely that scattering at energies much above 1 eV is important. This energy range is also convenient for a set of lectures since it naturally restricts the physical phenomena to a subset that can be described in a coherent manner.

A list of the relevant topics follow with references to some of the researchers shown in parenthesis:

* diffraction and ro-vibrationally inelastic dynamics from rigid surfaces
  - time independent quantum close coupling treatment (Wolken, Kouri)

- time dependent quantum wavepacket treatment (Kouri, Kosloff, Cerjan)
- semiclassical gaussian wavepacket treatment (Jackson & Metiu, Heller & Drolshagen)
- semiclassical trajectory treatment (Grote & DePristo, Toennies)

* interaction potentials for non-reactive scattering
  - smooth surfaces
  - corrugated surfaces

* quantum inclusion of surface atom motion (Jackson, Manson)

* classical generalized Langevin treatment of surface atom motion
  - formalism for harmonic solids (Adelman, Doll, Tully)
  - "ghost" atom reformulation (Tully, DePristo)
  - choice of parameters (Tully, DePristo)

* semiclassical stochastic trajectory treatment
  - 1 electronic channel (Richard, Lee, Geiger, DePristo, Clary)

* electron-hole pair processes (Billing, Newns, Metiu, Gadzuk, Gerber)

* examples
  - H_2 diffraction plus rotational excitation (Sibener, Kouri, Metiu)
  - CO_2 rotational and vibrational relaxation (Clary, Geiger, DePristo)
  - NO/Ag scattering (Zare, Auerbach, Rettner, Ertl, Asada, Tully)
  - NH_3/Au and HCl/Au (Kay)

* reactions at surfaces
  - precursor
  - direct
  - charge transfer model (Holloway, Gadzuk)
  - classical trajectory treatment (Thompson,Raff,Lee, Kara, DePristo)

* interaction potentials for dissociative chemisorption reactions
  - atom-surface chemisorption and embedding functions (Lee,Kara, DePristo)
  - LEPS formulation (Wolken,Lee,DePristo)
  - use of switching functions (Billing)

* examples
  - H_2 dissociation of Ni and Cu (Lee, Kara, DePristo)
  - N_2 on W (Kara, DePristo)
  - CO_2/Ni (Lee, DePristo)
  - CO_2/Pt (Billing)
  - experimental results on N_2/Fe, N_2/W, CH_4/Ni, H_2/Ni (Rettner, Auerbach, Ceyer, Ertl, Madix)

Due to the extensive nature of this list, I will not provide an even coverage of the topics.

I shall begin with the treatment of diffraction and ro-vibrationally

inelastic scattering from rigid surfaces. Neglect of surface atom motion is rather severe unless the mass of the impinging molecule is much less than that of the solid's atoms. For solids in the third row, this limits the treatment to H_2 and perhaps D_2.

The solid is assumed to have perfect 2D periodicity described by the surface reciprocal lattice vectors G_x and G_y. The fundamental quantum feature of the scattering is the change of the linear momentum of the scattered molecule by integer multiples of these lattice vectors. This is simply the result of the scattering of a wave from a periodic array. Let the initial and final momenta of the center of mass of the molecule be $\hbar\mathbf{k}$ and $\hbar\mathbf{k}_f$ with the two dimensional components in the surface plane being $\mathbf{K}$ and $\mathbf{K}_f$, respectively. The internal energies are ϵ_i and ϵ_f, respectively. Then conservation of energy and linear momentum yield:

$$k_f^2 + 2m\epsilon_f/\hbar^2 = k^2 + 2m\epsilon_i/\hbar^2 \qquad (1.1)$$

$$\mathbf{K}_f = \mathbf{K} + \mathbf{G}_{mn} \qquad (1.2)$$

where $\mathbf{G}_{mn}$ are two dimensional reciprocal lattice vectors. Such equations describe only the kinematics of the scattering since they are independent of the interaction between the molecule and the solid.

The Hamiltonian is simply

$$H = T(\underline{r}) + h(\underline{r}_i) + V(\underline{r},\underline{r}_i) \qquad (1.3)$$

where $\underline{r}=(x,y,z)$ specifies the position of the center-of-mass (CM) of the gas molecule and $\underline{r}_i$ denotes the internal molecular coordinates. $T(\underline{r})$ is the kinetic energy operator for the CM motion; $h(\underline{r}_i)$ is the hamiltonian for the internal motion of the free molecule; and, $V(\underline{r},\underline{r}_i)$ is the interaction potential between the molecule and the surface. Since the surface is rigid, V depends only upon $\underline{r}$ and $\underline{r}_i$. Furthermore, the 2D periodicity in

the potential implies the following expansion:

$$V(\underline{r},r_1) = \Sigma\, V_{mn}(z,r_1)\, \exp(i\underline{G}_{mn}\cdot\underline{R}) \qquad (1.4)$$

where $\underline{R}=(x,y)$ specifies the two dimensional components of $\underline{r}$ in the surface plane. It is the periodicity in Eq.(1.4) which distinguishes molecule-surface scattering from molecule-molecule scattering for example.

The wavefunction is also expanded in products of 2D Bloch waves and internal wavefunctions,

$$\Phi(\underline{r},r_1) = \Sigma\ \exp(i(\underline{K}+\underline{G}_{mn})\cdot\underline{R})\ \phi_j(r_1)\ g(z;m,n,j) \qquad (1.5)$$

Substitution of Eq.(1.5) into the time-independent Schrodinger equation, and use of orthogonality for both the 2D Bloch wavefunctions and the ϕ_j yields the set of close coupled equations to be solved for the unknown z-dependent functions $g(z;m,n,j)$:

$$[d^2/dz^2 + [\underline{d}^2]_{mnj}]g(z;m,n,j) - (2m/\hbar^2)\ \Sigma\ V(z;m,n,j,m',n',j')g(z;m',n',j') = 0 \qquad (1.6)$$

$$[\underline{d}^2]_{mnj} = (2m/\hbar^2)(E-\epsilon_j) - (\underline{K}+\underline{G}_{mn})^2 \qquad (1.7)$$

$$V(z;m,n,j,m',n',j') = \langle\phi_j,\underline{G}_{mn}|\ V(\underline{r},r_1)\ |\phi_{j'},\underline{G}_{m'n'}\rangle/A \qquad (1.8)$$

where A is the area of the unit cell. It is only necessary to specify the boundary conditions to finish the theoretical description. The initial wavefunction (as $z\to\infty$ with $\underline{k}\cdot\hat{z}<0$) is simply an incident plane wave in $\underline{r}$ times a specific molecular internal wavefunction:

$$\Phi_o(\underline{r},r_1) = \exp(i\underline{k}\cdot\underline{r})\phi_j(r_1) \qquad (1.9)$$

where the initial internal molecular wavefunction is ϕ_j. The final wavefunction is given as $z\to\infty$ with $\underline{k}\cdot\hat{z}>0$, by

$$g(z;m',n',j') \to (d_{m'n'j'})^{-\frac{1}{2}}\exp(id_{mnj}z)\delta_{m'n'j',mnj} + (d_{m'n'j'})^{-\frac{1}{2}}\exp(id_{m'n'j'}z)\ S(j',m',n'<-m,n,j) \qquad (1.10)$$

which defines the scattering or S-matrix. The particular definition in

Eq.(1.9) ensures that all the diffraction information is contained in the elements $S(j',m',n'<-0,0,j)$. Hence only one column of the S-matrix, for each $j'<-j$, is of interest for diffraction. In general however, all columns must be solved for in this close-coupled set of differential equations since that is the only way to ensure satisfying the proper boundary conditions.

It is currently possible to solve such sets of CC equations with high accuracy and numerical efficiency for perhaps a few hundred equations, with the computational time increasing like N_{eq}^3. If many calculations are required, as in adjustment of a PES for comparison to experimental data, fewer coupled equations can be handled. To get an idea of how many equations enter in a typical problem, consider H_2/Ni(100) scattering and assume that no asymptotically closed channels must be retained. Then, the number of coupled equations is specified by $[\underline{d}^2]_{mnj}>0$. With E=0, m=2 amu, E~.1 eV, $G_{mn}=(m,n)2\pi/2.49$ Å, $\epsilon_j=.00744j(j+1)$ eV, we find $(\hbar G_{10})^2/2m=0.00665$ eV and thus that for $j=0$, all $(m,n)=(0,0),(1,0),(1,1),(2,0),(2,1),(2,2),(3,0),(3,1),(3,2)$, are allowed, and for $j=2$ all $(m,n)=(0,0),(1,0),(1,1),(2,0),(2,1),(2,2)$ are allowed. Taking into account the symmetrical terms (-1,-1), (0,2) etc., we find the number of (m,n) channels is 1,4,4,4,8,4,4,8,8 for the $j=0$ terms listed and 1,4,4,4,8,4 for the $j=2$ terms listed. Taking into account that each $j=2$ rotational state is split into 5 m_j levels we find that there are 45+125=170 coupled equations. This number will decrease at lower E and higher incident angles. While symmetry can be used to lower the 170 dramatically in this case, it is clear that quantum CC approaches are inherently limited in the types of problems which can be treated.

A different type of quantum approach eliminates the use of a basis set entirely [4,7,8]. One starts with a wavepacket, $\Phi(\underline{r},\underline{r}_i)$, which is localized at large z and with an average velocity directed towards the surface. The time dependent Schrodinger equation is then solved over a short time interval $[t,t+\Delta t]$ via

$$\Phi(t+\Delta t;\underline{r}',\underline{r}_i') = \int \langle \underline{r}',\underline{r}_i'|exp(-iH\Delta t/\hbar)|\underline{r},\underline{r}_i\rangle\, \Phi(t;\underline{r},\underline{r}_i)\, d\underline{r}\, d\underline{r}_i \quad (1.11)$$

or via simpler finite difference evaluation in time. To see how the evaluation of the operator in the exponential is accomplished, we use a simpler notation suppressing the dependence upon r_i. Then a short time propagator is assumed, (i.e. using $[T,V]=0$), yielding

$$exp(-iH\Delta t/\hbar) \approx exp(-iT\Delta t/\hbar)\, exp(-iV\Delta t/\hbar) \quad (1.12)$$

Now T is a local operator in momentum space while V is local in coordinate space. Putting a complete set of states $|\underline{k}\rangle\langle\underline{k}|$ in obvious places we find

$$\Phi(t+\Delta t;\underline{r}') = \int \langle \underline{r}'|\underline{k}\rangle\langle\underline{k}|exp(-iT\Delta t/\hbar)|\underline{k}\rangle\langle\underline{k}|\underline{r}\rangle\langle\underline{r}|exp(-iV\Delta t/\hbar)|\underline{r}\rangle \Phi(t;\underline{r})\, d\underline{k}\, d\underline{r} \quad (1.13)$$

The transformations between coordinate and momentum space is accomplished via the fast fourier transform (FFT) algorithm. This transforms the coordinate space evaluation of $exp(-iV\Delta t/\hbar)\Phi(t)$ into momentum space; then the effect of $exp(-iT\Delta t/\hbar)$ is determined in this space to yield the momentum space wavefunction at $t+\Delta t$; and, finally the momentum space wavefunction function is transformed back to coordinate space via another FFT. Proceeding to the next time step, this procedure eventually yields the wavefunction as $t\to\infty$ from which all scattering information can be extracted via projections onto plane waves.

A number of advantages can be attributed to such a time-dependent wavepacket approach. First, it allows computation of only one column of

the S-matrix, exactly what is needed. Since a wavepacket is built from a number of translational energy eigenstates, this one column can be determined for a number of energies in a single calculation. Second, the method can be applied to non-rigid surfaces by including a time-dependent classical motion for the surface atoms. Third, the method is applicable to non-periodic surfaces. The major limitation is computational: the time is proportional to $N_g \ln N_g$ where N_g is the number of grid points used in the evaluation of the FFT. Assuming for simplicity an even grid in each degree of freedom and using a low number of grid points of 2^4=16, then in M-degrees of freedom we have $N_g=16^M$ which limits current treatments to M≤3 on current supercomputers unless only a single calculation must be performed in which case M=4 may be feasible. However, even a rigid rotor-rigid surface collision entails M=5 so that the FFT approach is really only applicable to atom-surface scattering. However, in that case it should provide much more capabilities than the standard time-independent scattering theory presented previously.

Before leaving the simplest type of molecule-surface collision system, I will mention something about the interaction potential, $V(\underline{r},\underline{r}_i)$. For simplicity, I will ignore the structure of the surface for now. Only the term $V_{00}(z,\underline{r}_i)$ in Eq.(1.4) enters then. At far distances from the surface, the molecule-surface interaction is a van der Waal's attraction, proportional to z^{-3}. At close distances, the overlap of the electronic distributions of the molecule and the surface leads to a repulsive interaction due to kinetic energy repulsion. For a non-reactive PES, the dependence of these interactions on the molecular bond length variation is quite weak, indicating that only the z and $\cos\theta=\hat{\underline{r}}_i\cdot\hat{\underline{z}}$ dependence are

important. The angular dependence is conveniently represented in a Legendre series:

$$V(z,\theta) = \Sigma\, V_l(z)\, P_l(\cos\theta) \qquad (1.14)$$

where the terms with $l>0$ give rise to rotational transitions. The more anisotropic the molecule solid PES, the larger the number of terms that must be retained in the expansion. The anisotropy in the long-range z^{-3} term can be determined from the anisotropy in the molecular polarizability but the anisotropy at short-range is much more difficult to get.

For the H_2/Cu system, I show in Figure 1.2 a reasonable PES with two terms retained in the expansion of Eq.(1.14). Two different short range anisotropic terms are considered, and these will give rise to very different amounts of rotationally inelastic scattering (look at the ratio of V_2/V_0 up till the classical turning point at .1-.15 eV).

One method to determine the corrugated, $(m,n)>(0,0)$, terms in the full PES involves simply assuming that higher terms are proportional to the (0,0) term. More sophisticated yet is the idea of using different proportionalities for the long and short range parts separately, since it is unlikely that the long-range term varies significantly with position in the unit cell. The best determined potentials use many parameters in the PES form, and fit to accurate scattering data, but this is really only been done for atom scattering from rigid surfaces. I will have much more to say about the much more complex reactive PES for dissociative chemisorption later.

(10a)

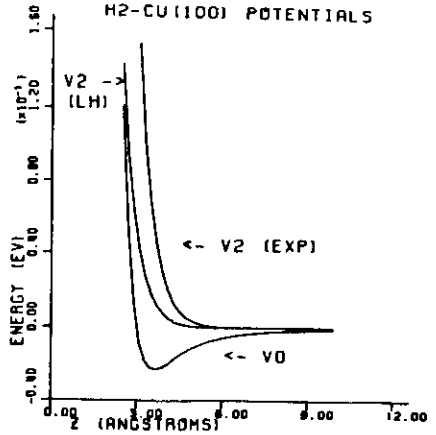

Fig. 2. Interaction potential for H_2–Cu(100) defined by eqs. (8a)–(8c) in the text. $\beta_s = 0.08$ for the LH potential and $\beta_s = 0.29$ for the EXP potential.

$$V_0(Z) = 267.60\, e^{-2.6267 Z} - 0.667/(Z-1.1225)^3$$

$$V_2(Z) = 267.60\, \beta_s\, e^{-2.6267 Z} - 0.05 \times 0.667/(Z-1.1225)^3$$

Figure 1.2

REFERENCES:

1. F. O. Goodman and H. Y. Wachman, "Dynamics of Gas Surface Scattering", (Academic Press, 1976).

2. G. Wolken, Jr. in "Dynamics of Molecular Collisions part A", ed. W. H. Miller (Plenum, 1976).

3. J. A. Barker and D. J. Auerbach, Surf. Sci. Reports 4 (1984) 1.

4. R. B. Gerber, "Molecular Scattering from Surfaces: theoretical methods and results", Chemical Reviews (1988).

5. "Dynamics of Molecule-Surface Interactions", Israel J. Chem., vol. 22 No. 4, pp. 283-413, eds. R. B. Gerber and A. Nitzan.

6. B.J. Garrison and N. Winograd, Science 216 (1982) 805.

7. R. B. Gerber, R. Kosloff and M. Berman, Computer Physics Reports 5 (1986) 59.

8. R. C. Mowrey and D. J. Kouri, J. Chem. Phys. 84 (1986) 6466.

9. A. E. DePristo, C. Y. Lee and J. M. Hutson, Surf. Sci. 169 (1986) 451.

MOLECULE-SURFACE SCATTERING: II

In this lecture, I shall consider the problem of inclusion of the motion of the solid's atoms. Formalisms for the quantum treatment of phonon events have been developed but these are limited in applicability to low energy processes and light gas molecules, for which single quantum events are the only important process. The most general fully quantum treatment (using path integrals and influence functionals) has not been developed or implemented to a significant degree.

I will introduce the most common method for the treatment of surface atom motion in collision processes, at least within a classical mechanics description. The basic physical idea is rather simple: the colliding molecule interacts strongly with a few close solid's atoms which then interact less strongly with their own neighbors and so forth. Eventually, the energy exchange between the gas molecule and a few strongly interacting solid's atoms in the initial collision is dissipated throughout the entire infinite solid.

The difficulty is describing the exchange of energy between the localized and extended system. While a simple brute force procedure is always capable of arbitrary accuracy if enough atoms are followed using molecular dynamics, such an approach may not be feasible for complex events which require thousands of molecular dynamics calculations to ensure statistically reliable results. Besides, this would not be a very intelligent use of computational resources.

To make progress, we note that while the motion of the strongly perturbed solid atoms will sample anharmonic forces from the other solid's atoms, the less strongly perturbed can be described by simple harmonic

restoring forces. In fact, I define a less strongly perturbed solid atom as one that can be described by harmonic restoring forces. Furthermore, the PES between the impinging molecule and the solid will be rather short ranged, and thus will not affect the less strongly perturbed solid atoms directly.

With the above ideas in mind, we focus on a harmonic solid, following closely the derivation due to Tully [1] based upon early work by Adelman and Doll [2] and even earlier by Zwanzig [3]. The equations of motion are

$$m_\alpha d^2 r_{\alpha i}/dt^2 = - \Sigma\, k(\alpha i,\beta j)\ (r_{\beta j}-r_{\beta j}^{o}) \qquad (2.1)$$

where m_α and r_α are the mass and position of the α^{th} solid atom, with $i=1,2,3$ the three cartesian directions. $k(\alpha i,\beta j)$ is the force constant for a distortion of the α^{th} atom in the i^{th} direction and the β^{th} atom in the j^{th} direction. $r_{\beta j}^{o}$ is the equilibrium position for the j^{th} direction and the β^{th} atom. Define mass-weighted displacement coordinates,

$$(\underline{u})_{\alpha j} = m_\alpha^{1/2}\ (r_{\beta j}-r_{\beta j}^{o}) \qquad (2.2)$$

and a frequency matrix,

$$(\underline{\Omega}^2)(\alpha i,\beta j) = k(\alpha i,\beta j)/(m_\alpha m_\beta)^{1/2} \qquad (2.3)$$

and use these to rewrite Eq.(13) in the matrix-vector notation:

$$d^2\underline{u}/dt^2 = - \underline{\Omega}^2 u \qquad (2.4)$$

Eq.(2.4) is now partitioned into two sets, one for N_P primary atoms and the other for N_S secondary atoms. This is done via the definitions $\underline{y}=\underline{P}\underline{u}$, $\underline{z}=\underline{Q}\underline{u}=(\underline{1}-\underline{P})\underline{u}$, $\underline{\Omega}^2_{PP}=\underline{P}\underline{\Omega}^2\underline{P}$, etc. with the result:

$$d^2\underline{y}/dt^2 = - \underline{\Omega}^2_{PP}\underline{y} - \underline{\Omega}^2_{PQ}\underline{z} \qquad (2.5)$$

$$d^2\underline{z}/dt^2 = - \underline{\Omega}^2_{QP}\underline{y} - \underline{\Omega}^2_{QQ}\underline{z} \qquad (2.6)$$

The idea is to eliminate the large set of $\underline{z}$, at least formally. This can be accomplished by solution of Eq.(2.6) for the secondary atom motion

and substitution of this solution into Eq.(2.5). The result is the fundamental integro-differential equation for the time evolution of the primary zone atoms within the generalized Langevin equation (GLE) approach:

$$d^2\underline{y}/dt^2 = - \underline{\Omega}^2_{PP}\underline{y} + \underline{M}(0)\underline{y}(t) - \underline{M}(t)\underline{y}(0) - \int \underline{M}(t-t')d\underline{y}(t')/dt'\ dt' + \underline{R}(t) \qquad (2.7)$$

The memory function and random force are defined by:

$$\underline{M}(t) = \underline{\Omega}^2_{PQ}\cos(\underline{\Omega}_{QQ}t)\underline{\Omega}_{QQ}^{-2}\underline{\Omega}^2_{QP} \qquad (2.8)$$

$$\underline{R}(t) = -\underline{\Omega}^2_{PQ}\cos(\underline{\Omega}_{QQ}t)\underline{z}(0) - \underline{\Omega}^2_{PQ}\sin(\underline{\Omega}_{QQ}t)d\underline{z}(0)/dt \qquad (2.9)$$

The memory kernel in Eq.(2.7) involves the response of the full many body system and thus retains 'memory" of previous velocities. This is distinct from a standard Langevin type equation which replaces the memory function by a δ-function and thus a local friction. The random force, $\underline{R}(t)$, and the memory kernel obey the fluctuation dissipation theorem:

$$\langle\underline{R}(t)\underline{R}(0)^T\rangle = kT\underline{M}(t) \qquad (2.10)$$

where the $\langle\rangle$ indicate an average over initial conditions of the secondary atoms. The derivation of Eq.(2.10) uses the equilibrium properties:

$$\langle\underline{z}(0)\underline{z}(0)^T\rangle = kT\underline{\Omega}_{QQ}^{-2} \qquad (2.11a)$$

$$\langle d\underline{z}(0)/dt\ d\underline{z}(0)^T/dt\rangle = kT\underline{1} \qquad (2.12b)$$

Eqs.(2.7-2.10) are equivalent to the original set of molecular dynamics equations in Eq.(2.4) or (2.5-2.6) in their ability to mimic an infinite solid. It appears that the GLE equations are limited in one sense: they cannot resolve energy transfer into the individual modes of the extended solid. But, this is not true since $\underline{z}(t)$ is given in terms of $\underline{y}(t)$ by the solution of Eq.(2.6). However, the GLE equations are no easier to solve in their present form since evaluation of $\underline{M}(t)$ and $\underline{R}(t)$ via Eqs.(2.8-2.9) is clearly impractical since the length of the Q-vectors is $3N_S$, which must be

quite large to simulate the bulk solid correctly. In addition, evaluation of a convolution integral with a general time dependence in the kernel is also impractical. Diagonalizing $\underline{\Omega}_{QQ}$ to $\underline{\tau}$, rewriting $\cos(\tau_i t)$ as separable exponentials and accruing integrals of the form

$$\int \exp(\tau_i t')d\underline{x}(t')/dt'\,dt'$$

is not practical since $6N_S$ such integrals must be accumulated even before doing all the multiplications in Eq.(2.8).

What is then the advantage of the GLE approach since it is no easier to solve the exact GLE equations than the original MD equations? The answer is that it is rather easy to approximate the memory kernel and random force to provide a reasonably accurate description of both the short time and long time (actually long wavelength) response of the primary zone atoms to an external perturbation (e.g. a collision). I will discuss this more fully in a while, but it is worthwhile to provide a more concrete answer, which will depend upon the precise application and accuracy that is important for the dynamics. If a truly quantitative description of the motion of the surface atoms is needed, then the GLE is really not the method of choice. One must resort to full MD with an accurate interatomic potential describing the solid's atoms, adding in perhaps some local frictional and random forces on the edge atoms to eliminate reflection of energy from the edge of the MD zone. At the other extreme, if a simple qualitative picture of the effect of solid atom motion is needed, then the GLE is much too complex and one should utilize simple models such as the soft cube. Most collision problems do not fall into these extremes. The PES is not know accurately enough to warrant an extremely accurate treatment of the surface atom motion, and one is generally not interested

in knowing the precise percentage of energy loss to the lattice. However, it is important to know whether 10%, 50% or 90% of the molecule's energy is transferred to the lattice, etc. Thus, almost all realistic simulations of molecule-surface collision dynamics should utilize a GLE prescription for the motion of the solid's atoms. However, I will qualify this statement a little later.

I now describe the common approximation to the memory function [1,4]. One expects a decaying and oscillating function on physical grounds. Using

$$\underline{M}(t)=\underline{M}_0^{\frac{1}{2}}\exp(-\underline{\tau}t)[\cos(\underline{w}_1 t)+\tfrac{1}{2}\underline{\tau}\underline{w}_1^{-1}\sin(\underline{w}_1 t)]\underline{M}_0^{\frac{1}{2}} \qquad (2.12)$$

which is the multidimensional generalization of the position autocorrelation function of a Brownian oscillator provides such a function with a number of unknown parameters. Forcing Eqs.(2.8) and (2.12) and their second time derivatives to agree at t=0 (the first time derivative vanishes identically), yields a set of equations for the unknown coefficient matrices [4]:

$$\underline{M}_0 = \underline{\Omega}^2_{PQ}\underline{\Omega}_{QQ}^{-2}\underline{\Omega}^2_{QP} \qquad (2.13)$$

$$\underline{M}_0^{\frac{1}{2}}\underline{w}_o^2\underline{M}_0^{\frac{1}{2}} = \underline{\Omega}^2_{PQ}\underline{\Omega}^2_{QP} \qquad (2.14)$$

where

$$\underline{w}_o^2 = \underline{w}_1^2+\tfrac{1}{4}\underline{\tau}^2 \qquad (2.15)$$

The exponential decay parameter is chosen to produce the correct long-wavelength limit for the density of states,

$$\underline{\tau} = \pi w_b \underline{1}/6 \qquad (2.16)$$

where w_b is the bulk Debye frequency.

An alternate procedure due to Tully [1], and which preceded the above method, is to choose the elements of the parameter matrices to duplicate the phonon spectrum of the crystal. This spectrum is related to the

fourier cosine transform of the velocity autocorrelation function for a monatomic fcc crystal. After considerable algebra, it can be shown that:

$$g(w) = kTw^2 \tau \underline{AUBU}^T \underline{A} \qquad (2.17)$$

where $g(w)$ is the density of states at frequency w. This is a projection onto each atom. The new matrices in Eq.(2.17) are

$$\underline{A} = (w^2\underline{1} - \underline{\Omega}^2_{PP})^{-1} \qquad (2.18)$$

$$\underline{B} = (w^2\underline{\tau}^2 + (\underline{U}^T\underline{AU} + \underline{w}_o^2 - w^2\underline{1}))^{-1} \qquad (2.19)$$

The two methods for choice of the parameters will agree if an accurate full force constant matrix, $k(\alpha i, \beta j)$, or frequency matrix, $\underline{\Omega}$, are available. If not, then it is a matter of convenience which method is preferable. Either one will capture the essential features of the GLE, namely frictional energy loss from the primary atoms to the secondary atoms and thermal energy transfer from the secondary atoms to the primary atoms. And both will provide a reasonable description of the bulk and surface phonon density of states of the solid. This is illustrated in Figure 2.1 where a LJ(12,6) model of an FCC crystal is used to generate $\underline{\Omega}$; in Tully's method, a lower surface normal frequency component was chosen but in any case the agreement between the methods is reasonable. Neither will provide the exact time dependent response of the solid due to the limited number of parameters used to describe the memory function.

The approximate memory function in Eq.(2.12) allows for a replacement of the GLE Eq.(2.7) by

$$d^2\underline{Y}/dt^2 = -\underline{\Omega}^2_{PP}\underline{Y} + \underline{M}_0^{-\frac{1}{2}}\underline{w}_o\underline{z} \qquad (2.20)$$

$$d^2\underline{z}/dt^2 = \underline{w}_o\underline{M}_0^{-\frac{1}{2}}\underline{Y} - \underline{w}_o^2\underline{z} - \underline{\tau}d\underline{z}/dt + \underline{f}(t) \qquad (2.21)$$

where $\underline{f}(t)$ is a gaussian white noise random force. The fictitious particles obeying the equations of motion of $\underline{z}$ are commonly referred to as

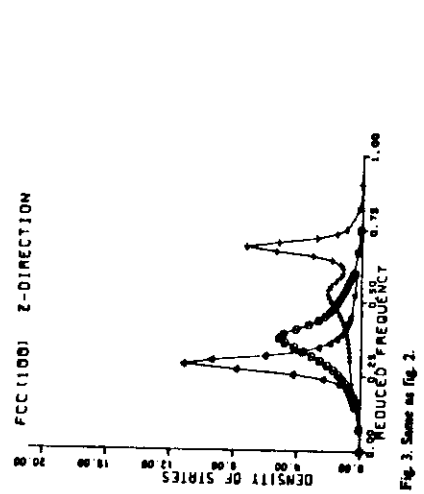

Fig. 3. Same as fig. 2.

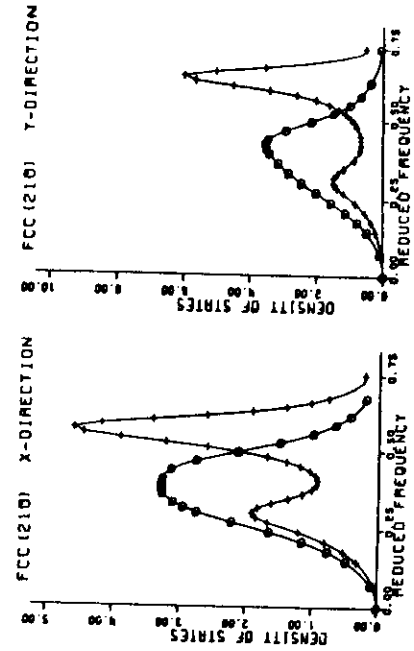

Fig. 4. Fourier cosine transforms of the velocity autocorrelation function versus frequency in units of w_D. Values are shown for the first surface atom (O) and first subsurface atom (+). The positions of the atoms are shown in table 1 and fig. 1. All curves are normalized to unit area.

Fig. 5. Same as fig. 4.

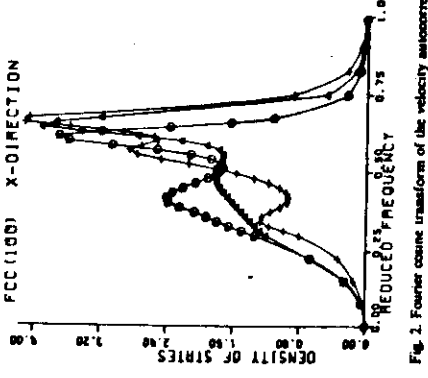

Fig. 2. Fourier cosine transforms of the velocity autocorrelation functions versus frequency in units of w_D. Values are shown for the first surface atom (O) and first subsurface atom (+). The results using the parameters in ref. [7] are also shown for the first surface atom (o). The positions of the atoms are shown in table 1 and fig. 1. All curves are normalized to unit area.

Surf. Sci. 91 (1980) 40.

J. C. Tully, J. Chem. Phys. 73 (1980) 1975.

Figure 2.1 : Parameterization of Tully's GLE-ghost atom formulation.

(6a)

a "ghost" atoms, and thus this formulation is referred to as the GLE-"ghost" atom method.

To emphasize the physics again for this method, I note that the harmonic restoring force, $-\underline{\Omega}^2_{pp}\underline{x}$, provides the interaction among the primary zone atoms. The coupling between the primary and "ghost" atoms is incorporated by the terms $\underline{M}_0^{\frac{1}{2}}\underline{w}_o\underline{s}$ and $\underline{w}_o\underline{M}_0^{\frac{1}{2}}\underline{x}$. The frictional force, $-\underline{\gamma}d\underline{s}/dt$, and the gaussian random force are related via a simpler fluctuation dissipation than in Eq.(2.10):

$$\langle \underline{f}(t)\underline{f}(0)^T \rangle = 2kT\underline{\gamma}\delta(t) \qquad (2.22)$$

where $\delta(t)$ is a Dirac delta function. This balance ensures that in the long time limit, the positions and velocities for the primary and "ghost" atoms become thermally distributed at a temperature T.

Finally, I want to note a few points about the GLE formalism. First, it is easy to remove the assumption of harmonic interactions among the primary atoms simply by replacing $-\underline{\Omega}^2_{pp}\underline{x}(t)$ in Eqs.(2.7) or (2.20) by the exact forces. This does not cause any difficulties with any of the other equations. But, it is not possible to implement a GLE in any practical way if the primary-secondary or secondary-secondary interactions are anharmonic. Second, a complication arises within the GLE formalism due to the localized nature of the primary zone atoms. In a molecule-surface collision, the initial localized interaction specifies a set of primary zone atoms, but when the molecule moves over the surface, a new set of primary zone atoms must be defined. This process is called switching of the primary zone and is illustrated in Figure 2.2. However, there is no a-priori method to consistently define a new primary zone atoms since there is no information on the flow of energy from the original primary zone into

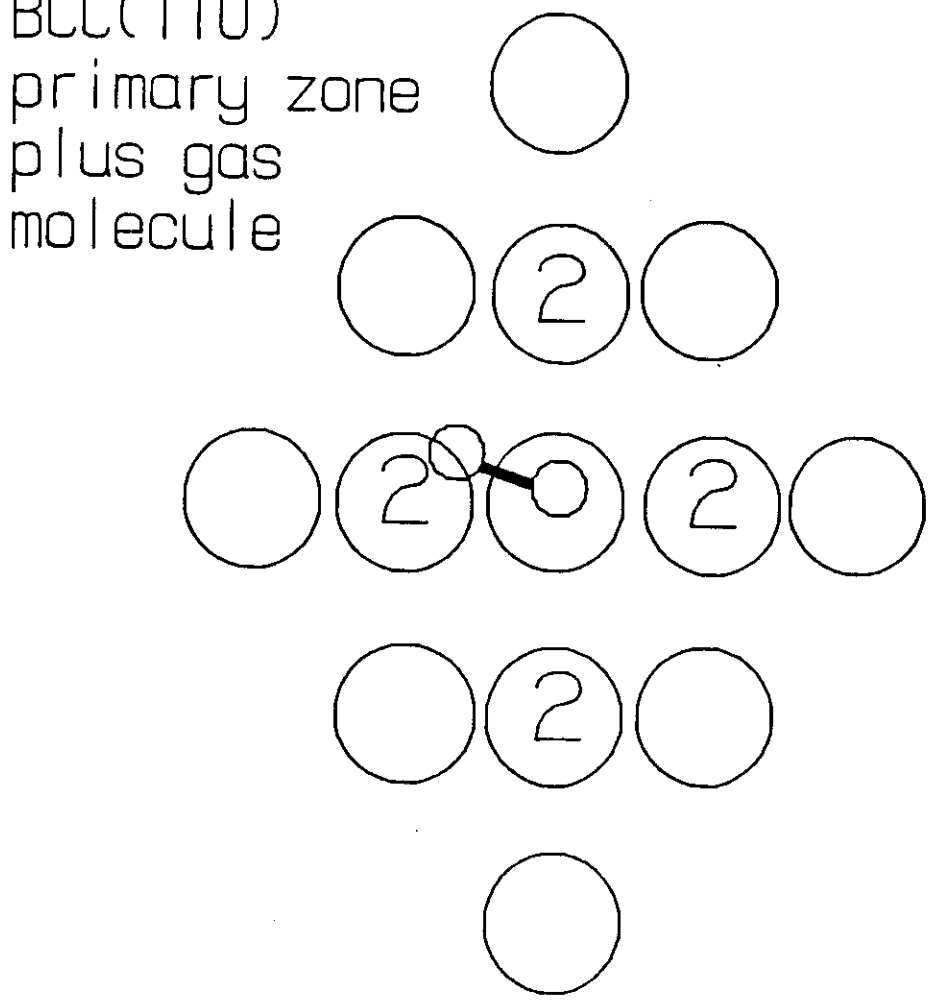

Figure 2.2

the specific secondary zone atoms (i.e. the exact $\underline{H}(t)$ is no longer available). The currently used assumption is that the motion of the molecule across the surface is slow compared to thermalization of the surface atoms. Then the new primary zone atoms are reinitialized from a thermal distribution. Such a method will break down if the motion of the molecule is very fast and/or the distortion of the lattice is sufficiently great to inhibit thermalization on a fast enough time scale.

Before leaving this subject, I wanted to note that the GLE is not a particularly simple method to implement. One must choose the parameters, which will differ for each surface face and material, a procedure which is intensive of human time. Changing the number of primary zone atoms requires redetermination of these parameters, and major modifications of a computer code to implement the switching process. If a treatment of a particular material and surface face is to be focused on for an extended period of time, then the investment in human time is definitely worthwhile (especially if computational resources are limited.) If a number of faces and materials are to be treated, then still simpler methods combining GLE and MD are desirable, although more expensive computationally.

Now I will turn to a brief mention of the treatment of the other low energy excitation modes, namely electron-hole pair (denoted by e-h) creation and annihilation. It is my opinion that these will not be very important for translational to e-h pair processes since the coupling to phonons is so much stronger [5] as indicated in Figure 2.3. The exception may be atomic H and D [6]. The major role for e-h pair processes is likely in vibrational excitation and deexcitation for weakly interacting molecule-surface systems. First, let me emphasize that e-h pair processes are

distinct from the simple coupling of molecular and electronic degrees of freedom adiabatically. For example, if the molecular bond length varies as the molecule approaches a surface, the dynamics can effect translational to vibrational energy transfer and vice versa. This process should be relatively independent of the surface temperature. By contrast, experimental data [7] for the NO/Ag(111) system has shown that NO is vibrationally excited with a probability of the form

$$P = f(E_i\cos^2\theta_i)\exp(-E_a/kT) \qquad (2.23)$$

which indicates that at T=0K there is no vibrational excitation. On the other hand, the probabilities are quite small even at T=760K, increasing from .01 to .06 as $E_i\cos^2\theta_i$ increases from .01 eV to 1.2 eV as shown in Figure 2.4.

The treatment of such processes is provided by Newns [8] along the lines developed by others [9,10]. The starting point is the hamiltonian,

$$H = \epsilon_a(t)n_a + \Sigma\epsilon_k n_k + V(t)\Sigma(c_a^\dagger c_k + h.c.) + \nu_o b^\dagger b + rn_a(b^\dagger + b) \qquad (2.24)$$

$\epsilon_a(t)$ is the energy level of the π^* level in NO and is dependent upon the position of the CM of NO from the surface (z), which provides the time-dependence via motion of the NO CM, i.e. z=z(t). $n_a=c_a^\dagger c_a$ is the occupation number operator for this level. ϵ_k and n_k ~~are the~~ refer to the electronic eigenstates of the metal's electrons. V(t) is actually $V(z(t))=V^0\exp(-\alpha z(t))$, where z(t) is assumed to be known from motion on a PES. ν_o is the frequency of vibration in the NO and NO^-, assumed to be the same. The operator "b" annihilates a vibrational quanta in either NO or NO^-. The electron-vibration coupling within the molecule is provided by the last term in Eq.(2 24). Thus, this equation contains two types of electron-vibration coupling, that between the e-h pairs of the solid and

 Chem Phys. 116 (1987) 269.

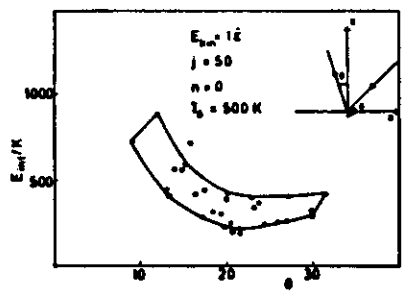

Fig. 3. Energy accomodation to the surface phonons as a function of scattering angle θ for CO scattered from a Pt(111) surface. The incident angles are $\theta = 45°$ and $\phi = 0°$. The surface temperature is T_s = 500 K, the kinetic energy 1 e (100 kJ/mol) and the initial vibrational and rotational angular momenta $(n, j) = (0, 50)$ (in units of $\hbar$). The final scattering angle ϕ is 180 ± 5°. We notice that the trajectories (marked by O) fall within a characteristic loop (run 3, table 1).

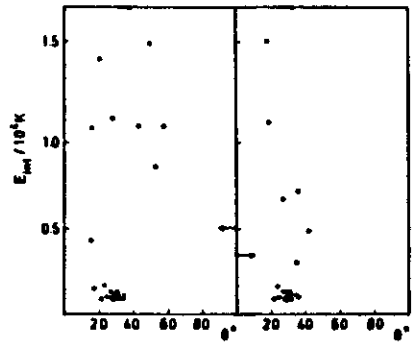

Fig. 4. Same as fig. 3 but for run 5 of table 1. Left panel shows the result obtained including phonon coupling only whereas the right panel shows the distribution if electron–hole pair excitation is included. The average energy transfer $\langle E_{vib} \rangle$ is also indicated. The energy-loss loops are less characteristic than in fig. 3 due to larger sticking probabilities (see runs 5 and 5* in table 1).

Figure 2.3

D.M. Newns, Surf Sci 171 (1986) 600.

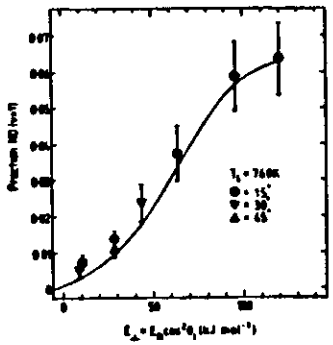

Fig. 5. Plot of $v = 1$ probability versus normal kinetic energy $E_\perp$ of NO beam. Points, experiment of ref. [7], curve, results of theory using data of table 1.

Figure 2.4

the π^* level of NO and that between vibrations of NO and NO$^-$ (i.e. $n_a = 1$).

Solution of Eq.(2.24) for the operator "b", and then determination of $n_a(t)$ by first order perturbation theory yields a formula similar to Eq.(2.23). A number of assumptions must be made to obtain quantitative agreement with experiment, including two critical ones. First, the spatial dependence of the location of the π^* energy level is written as

$$\epsilon_a(z) = \epsilon_a(\infty) - 1/4(z-z_o) \qquad (2.25)$$

Second, the lifetime broadening of the π^* level varies as

$$\Delta(z) = \Delta^0 \exp(-2\alpha z) \qquad (2.26)$$

The parameter z_o controls the effect of the coupling with distance out into the vacuum, since it changes the energy gap between the excited and ground electronic level. And, Δ^0 controls the rate of deexcitation from the π^* level. The particular values are z_o=-1.93 Å and $\hbar/\Delta^0 = 6x10^{-15}$ sec. The sensitivity to these values is in accord with a different approach based upon electronic friction terms, where the spatial extent of the electronic friction controlled the probability of energy dissipation to e-h pairs [11]. Finally, I might suggest a recent article by Billing [5] for further reading since it provides a more collision orientated approach to the treatment of e-h pair excitations for translational energy loss.

REFERENCES

1. J. C. Tully, J. Chem. Phys. 73 (1980) 1975.

2. S. A. Adelman and J. D. Doll, Acc. Chem. Res. 10 (1977) 378; S. A. Adelman, Adv. Chem. Phys. 44 (1980) 143 and references therein.

3. R. W. Zwanzig, J. Chem. Phys. 32 (1960) 1173.

4. A. E. DePristo, Surf. Sci. 141 (1984) 40.

5. G. D. Billing, Chem. Phys. 116 (1987) 269.

6. Z. Kirson, R. B. Gerber, A. Nitzan and M. A. Ratner, Surf. Sci. 137 (1984) 527.

7. C. T. Rettner, F. Fabre, J. Kimman and D. J. Auerbach, Phys. Rev. Lett. 55 (1985) 1904.

8. D. M. Newns, Surf. Sci. 171 (1986) 600.

9. B. N. J. Persson and M. Persson, Solid State Commun. 36 (1980) 175.

10. J. W. Gadzuk, J. Chem. Phys. 79 (1983) 6341; 81 (1984) 2828.

11. A. E. DePristo, C. Y. Lee and J. M. Hutson, Surf. Sci. 169 (1986) 451.

MOLECULE-SURFACE SCATTERING: III

With the GLE treatment of the lattice motion available, I now will turn to inclusion of surface atom motion into treatments of diffraction and inelastic scattering. The description of dissociative chemisorption dynamics will also utilize the GLE. In either case, the collision adds an additional force on the primary zone atoms, and adds a time scale over which the response of the solid is required, namely the collision time t_c (i.e. the duration of a "strong" interaction).

These GLE-"ghost" atom equations describe a set of coupled harmonic oscillators with damping and fluctuating forces. The rate of damping is determined by $|\underline{\tau}^{-1}|$ while the energy exchange between primary and "ghost" atom subsystems is controlled by $\underline{\omega}_o\underline{M}0^{\frac{1}{2}}$. Typically, these two time scales are very similar since they both reflect the motions of the solid's atoms which are controlled by the forces between solid atoms. The other relevant time scale is t_c. When $t_c<<|\underline{\tau}^{-1}|$, the solid response is limited to the motion of the primary zone atoms, with negligible effects due to the remainder of the solid, i.e. the "ghost" atoms. When $t_c\sim|\underline{\tau}^{-1}|$, the response of the solid is truly a <u>dynamical</u> many body phenomena since the energy exchange between the gas molecule and primary zone atoms is strongly influenced by the "ghost" atoms on the time scale of the collision duration. When $t_c>>|\underline{\tau}^{-1}|$, the solid responds as a many body <u>equilibrium</u> system, describable via a classical Langevin treatment without memory. This has also been described by a T-dependent potential of mean force [1]. We shall not consider such cases. For the reader's information, $|\underline{\tau}^{-1}|\sim 1.5\times10^{-11}$ K-sec/θ_D where θ_D is the Debye temperature. A typical range is 100 K < θ_D < 400 K, yielding 1.5×10^{-14} sec < $|\underline{\tau}^{-1}|$ < 3.5×10^{-14} sec. A

typical collision duration is 10^{-15} - 10^{-11} sec.

The most direct and accurate way to include energy transfer to the solid involves augmentation of the time dependent scattering theory in Eq.(1.11) to include a time dependent Hamiltonian [2,3]:

$$\Phi(t+\Delta t;\underline{r}',\underline{r}_1') = \int \langle \underline{r}',\underline{r}_1'|\exp(-iH(t)\Delta t/\hbar)|\underline{r},\underline{r}_1\rangle \Phi(t;\underline{r},\underline{r}_1)\, d\underline{r}\, d\underline{r}_1 \quad (3.1)$$

where

$$H(t)=T(\underline{r},\underline{r}_1) + V(\underline{r},\underline{r}_1,\underline{Y}(t),\{\underline{r}_\beta^o\}) \quad (3.2)$$

$\{\underline{r}_\beta^o\}$ are the fixed positions of all the solid's atoms and must be included since the PES will generally depend upon many more atoms than just those in the primary zone. In Eq.(3.2) I have neglected variations of $H(t)$ over the time Δt since the lattice atoms are much heavier and move much more slowly than the impinging gas molecule. The time dependence of $\underline{Y}(t)$ is calculated via the GLE-"ghost" atom formalism as presented in Lecture II, but with an additional force due to the interaction potential $V(\underline{r},\underline{r}_1,\underline{Y}(t),\{\underline{r}_\beta^o\})$. This can be done in a manner that would conserve energy in the absence of frictional and random forces, by using Ehrenfest's theorem:

$$d^2\underline{Y}/dt^2 = -\nabla_{\underline{Y}} V(\underline{Y},\{\underline{r}_\beta^o\}) - \underline{\Omega}^2 PP\underline{Y} + \underline{M}_0^{-\frac{1}{2}}\underline{w}_o\underline{s} \quad (3.3)$$

$$d^2\underline{s}/dt^2 = \underline{w}_o\underline{M}_0^{-\frac{1}{2}}\underline{Y} - \underline{w}_o^2\underline{s} - \underline{r}\,d\underline{s}/dt + \underline{f}(t) \quad (3.4)$$

where

$$V(\underline{Y},\{\underline{r}_\beta^o\}) = \langle \Phi(t;\underline{r},\underline{r}_1)|V(\underline{r},\underline{r}_1,\underline{Y}(t),\{\underline{r}_\beta^o\})|\Phi(t;\underline{r},\underline{r}_1)\rangle \quad (3.5)$$

This illustrates the power of the time dependent solution of the Schrodinger equation since the calculation of $\underline{Y}(t)$ and $\underline{s}(t)$ involves a relatively small amount of extra time over that due to simple evolution of $\Phi(t;\underline{r},\underline{r}_1)$ with a rigid surface. Even the evaluation in Eq.(3.5) is not particularly tedious since the wavefunction is already know on the grid of $(\underline{r},\underline{r}_1)$ values. However, for a non-zero T, the initial conditions of the

primary and "ghost" atoms must be sampled. This implies that a considerable number of $\Phi(t;\underline{r},\underline{r}_1)$ must be propagated and then averaged incoherently to determine the full wavefunction.

The above method is a specific illustration of the time dependent self-consistent field (TDSCF) approach [4-6]. In the TDSCF theory, a full wavefunction for two coordinates, X,Y is approximated via,

$$\phi(t;X,Y) = \Phi(t;X)\theta(t;Y) \quad (3.6)$$

and the full TDSE

$$[T(X)+T(Y)+V(X,Y)]\phi(t;X,Y) = i\hbar\partial\phi(t;X,Y)/\partial t \quad (3.7)$$

is replaced by the set of equations:

$$[T(X) + \langle\theta(t;Y)|V(X,Y)|\theta(t;Y)\rangle]\Phi(t;X) = i\hbar\partial\Phi(t;X)/\partial t \quad (3.8)$$

$$[T(Y) + \langle\Phi(t;X)|V(X,Y)|\Phi(t;X)\rangle]\theta(t;Y) = i\hbar\partial\theta(t;Y)/\partial t \quad (3.9)$$

Eqs.(3.8-3.9) are the best variational solution of Eq.(3.7) with the simple product wavefunction in Eq.(3.6). If the original Eq.(3.7) conserves energy then the TDSCF Eqs.(3.8-3.9) also conserve energy. The molecule-surface scattering description in Eqs.(3.1-3.5) results from the identification of $X\to(\underline{r},\underline{r}_1)$ and $Y\to(\underline{r}_\beta)$. Then, the addition assumption that the wavefunction for Y is peaked around the classical value, $Y(t)$, is used to replace the TDSE in Eq.(3.9) by Hamilton's equations. This then leads to the GLE-"ghost" atom formalism as presented in Lecture II.

It is of course possible to simplify the molecule-surface scattering problem further by simplification of solution of the TDSE part in Eq.(3.1). This is equivalent to implementation of the multitude of approximations that have been developed in gas phase scattering dynamics. For example, if the center-of-mass of the molecule is also assumed to follow a classical trajectory (i.e.$\Phi(t;\underline{r},\underline{r}_1)\approx\theta(t;\underline{r}_1)F(t;\underline{r})$ with $F(t;\underline{r})$ peaked around the

classical trajectory $\underline{X}(t)$), then the semiclassical stochastic trajectory (SST) approximation [7-9] results:

$$\theta(t;\underline{x}_1) = \Sigma\, c_k(t)\phi_k(\underline{x}_1)\exp(-i\epsilon_k t/\hbar) \tag{3.10}$$

$$dc_k(t)/dt = \Sigma\, \langle\phi_k(\underline{x}_1)|V(\underline{X}(t),\underline{x}_1,\underline{Y}(t),\{\underline{x}_\beta^o\})|\phi_j(\underline{x}_1)\rangle \exp(i[\epsilon_k-\epsilon_j]t/\hbar)\; c_j(t) \tag{3.11}$$

$$Md^2\underline{X}/dt^2 = -\nabla_{\underline{X}}V(\underline{X},\underline{Y},\{\underline{x}_\beta^o\}) \tag{3.12}$$

$$V(\underline{X},\underline{Y}(t),\{\underline{x}_\beta^o\}) = \langle\Phi(t;\underline{x}_1)|V(\underline{X},\underline{x}_1,\underline{Y},\{\underline{x}_\beta^o\})|\Phi(t;\underline{x}_1)\rangle \tag{3.13}$$

Note that a basis set expansion is not necessary but is implemented to retain close correspondence with the original derivation. I could just as well use the analog of Eq.(3.1) instead of Eqs.(3.10-3.11) to determine the time evolution of $\theta(t;\underline{x}_1)$. The advantages in either case is the reduction of the number of quantum degrees of freedom which must be treated explicitly. For example, in a diatomic molecule-surface collision treated as in Eqs.(1-3), there are 6 quantal degrees of freedom, which is too many for current computational facilities. However, using a SST technique there are only 3 quantal degrees of freedom, which is perfectly tractable using an FFT propagation method, for example. Equivalently, in a the basis set expansion Eq.(3.11), only a manageable set of basis functions are needed to span the rotation-vibration space.

The difficulty with the SST approach is the replacement of the correlation between translational and internal energies of each internal state with an correlation between the <u>average</u> translational energy and all the states. The physical implication is that the prediction of the internal energy or state distribution for a particular angle of the product scattering is not possible. Instead only the internal state distribution averaged over all final angles is provided. Although, this is a much more

severe limitation than that of separating molecular and phonon degrees of freedom in the TDSCF, the SST is much easier and faster to implement. Indeed, calculations of vibrational-rotational relaxation in CO_2/Pt collisions have been accomplished involving over 600 vibration-rotation states in the expansion [9].

It is possible to retain the correlation between internal and translational degrees of freedom by replacing the exact translational wavefunction by a simpler function that is nearly but not totally classical. This is the idea of gaussian wavepacket dynamics (GWD) [10-13], in which the full molecular wavefunction is expanded as:

$$\Phi(t;\underline{X},\underline{x}_1) = \Sigma\, c_{\alpha k}(t)\; [C_{\alpha k}G_{\alpha k}(t;\underline{X})]\; \phi_k(\underline{x}_1)\exp(-i\epsilon_k t/\hbar) \tag{3.14}$$

where each translational gaussian wavepacket is of the form

$$G_{\alpha k}(t;\underline{X}) = \exp\{(i/\hbar)[(\underline{X}-\underline{X}_{\alpha k}(t))\cdot\underline{\underline{A}}_{\alpha k}(t)\cdot(\underline{X}-\underline{X}_{\alpha k}(t)) + \underline{P}_{\alpha k}(t)\cdot(\underline{X}-\underline{X}_{\alpha k}(t))]\} \tag{3.15}$$

The index α exists because a linear combination of GWP must be formed to mimic an incident 2D plane wave, i.e. the $\underline{K}$ part of the initial wavefunction in Eq.(1.9). The coefficients $C_{\alpha k}$ are dependent on the index k only through the energy of the initial translational wavevector. The time-dependent coefficients $c_{\alpha k}(t)$ satisfy complicated differential equations, and the reader is referred to the original work [13]. The parameters in a gaussian wavefunction follow the (generic) equations of motion [10-13]:

$$d\underline{\underline{A}}/dt = -(2/m)\underline{\underline{A}}(t)\cdot\underline{\underline{A}}(t) - \underline{\underline{K}} \tag{3.16}$$

$$d\underline{X}/dt = (1/m)\underline{p}(t) \tag{3.17}$$

$$d\underline{p}/dt = -\nabla_{\underline{r}}\langle V\rangle \tag{3.18}$$

where $\underline{\underline{K}}$ is the matrix of expectations values of second derivative of V.

The difficulty with this approach is the very large number of coupled differential equations which arise for each wavepacket-internal state: 9 for the matrix $\underline{A}$, 3 for $\underline{r}$, 3 for $\underline{p}$, 1 complex for $c_{\alpha k}$. Since the $c_{\alpha k}$ couple all the wavepacket-internal state combinations, the total number of real differential equations is $17N_gN_i$ where N_g and N_i are the total number of wavepackets and internal states, respectively. A typical number is N_g=10-20 which implies that about $200N_i$ coupled differential equations result from this approach. This poses a rather intractable problem since it is nearly always true that $N_i>2$, with they typical case being that $N_i>10$.

To alleviate these problems, one may utilize a single translational function as in the TDSCF approach but not make the classical path approximation [12]. This replaces the multiple GWP expansion in Eq.(3.14) by the mean trajectory GWP method:

$$\Phi(t;\underline{r},\underline{r}_i) = F(t;\underline{r})\ \Sigma\ c_{\alpha k}(t)\phi_k(\underline{r}_i)\exp(-i\epsilon_k t/\hbar) \qquad (3.19)$$

where the single translational wavefunction is given by

$$F(t;\underline{r}) = \Sigma\ C_\alpha G_\alpha(t;\underline{r}) \qquad (3.20)$$

Each GWP propagates independently, leading to equations nearly identical to those of the SST method but supplemented by equations for the time evolution of the matrix $\underline{A}$. The RHS of the coefficient differential Eq.(3.11) has an added term of the form $-(1/2m)p_\alpha(t)\cdot p_\alpha(t)$ $-(i\hbar/m)Tr\underline{A}(t)$ and utilizes an average over the appropriate gaussian wavepacket. The advantage to this approach is the coherence of the superposition, which allows for the treatment of diffraction by the summation of GWP. However, it does not allow for any added correlation between the translational and internal degrees of freedom. In particular, it cannot be used to predict

the simultaneous angular and internal energy distributions, although it can be used to predict the former in the absence of any internal energy changes.

The basic problem with all of the methods which utilize some TDSCF approximation is this destruction of the correlation between internal and translational degrees of freedom, which would result from an accurate solution of Eqs.(3.1-3.2). The treatment of energy transfer with the lattice is in very good shape using the GLE-"ghost" atom formalism in Eqs.(3.3-3.5). Why then has there been so much work focused on such TDSCF and related approximations? It is the same reason that plagues all of dynamics: there are no general methods that can be used to treat more than 3 or at most 4 degrees of freedom via quantum mechanics. Hence, everyone is forced to develop simpler methods that allow some problems to be treated with some accuracy. But the real goal of treating these systems by consistent quantum mechanical solution remains an elusive one.

In contrast to the considerable difficulties with either a full quantum mechanical or semi-classical treatment, the implementation of a full classical treatment of molecule-surface dynamics is not really difficult (but could still require substantial computational time depending upon the complexity of the PES and its derivatives). The Newtonian equations provide an exact correlation between internal and translational degrees of freedom. The problem with classical treatments are not implementation but validity. Classical simulations eliminate or at best treat poorly the distinctly quantum mechanical processes such as diffraction, and quantized internal energies. Since I would like to describe the angular, translational and internal state distributions of the scattered molecules,

classical dynamics is not adequate unless these effects are negligible. However, for heavier molecules, especially when state-to-state vibrational transitions are not desired, a classical trajectory-GLE-"ghost" atom approach is probably perfectly adequate. This has the advantage of focusing attention on the <u>results</u> of the calculation and not on the calculation itself, precisely the way to understand real chemical and physical systems in my opinion.

Before considering some results, let me mention a possible solution to the implementation of quantum mechanics. Basically, I want to treat many quantum dynamical degrees of freedom, and shall denote these by the generic $\underline{x}$. We can rewrite Eq.(3.1) in the more explicit form:

$$\langle t';\underline{x}'|\Phi\rangle = \int \langle \underline{x}'|exp(-iH(t'-t)/\hbar)|\underline{x}\rangle\langle t,\underline{x}|\Phi\rangle\, d\underline{x} \qquad (3.21)$$

which indicates that the necessary quantity is the propagator

$$U(t',\underline{x}';t,\underline{x}) = \langle \underline{x}'|exp(-iH(t'-t)/\hbar)|\underline{x}\rangle \qquad (3.22)$$

For multi-dimensional problems, the only practical method to evaluate such a quantity is a path integral representation:

$$exp(-iH(t'-t)/\hbar) = [exp(-iH\delta t/\hbar)]^N$$

$$\delta t=(t'-t)/N$$

$$U(t',\underline{x}';t,\underline{x}) = \int \langle \underline{x}'|exp(-iH\delta t/\hbar)|\underline{x}_1\rangle\langle \underline{x}_1|exp(-iH\delta t/\hbar)|\underline{x}_2\rangle\ldots$$

$$\langle \underline{x}_{N-1}|exp(-iH\delta t/\hbar)|\underline{x}\rangle\, d\underline{x}_1\ldots d\underline{x}_{N-1} \qquad (3.23)$$

By making each N large enough and each time interval $t'-t$ small enough, each effective short time propagator $\langle \underline{x}_i|exp(-iH\delta t/\hbar)|\underline{x}_{i+1}\rangle$ is approximated via use of some commutivity assumption $[T,V]=0$. Then, the multidimensional integrals over $(\underline{x}_i,\ i=1,\ldots,N-1)$ are performed via Monte-Carlo methods. Even very quantum degrees of freedom for nuclear motion are unlikely to require more than 10-20 intermediate paths or expansion states. Thus a

quantum system with N_Q degrees of freedom maps onto a classical like Monte Carlo system with $\approx 10N_Q$ degrees of freedom. This would allow for easy evaluation of even N_Q=100. The bottleneck is the evaluation of an oscillatory function via Monte Carlo methods since exp(iF) does not provide a positive definite sampling function. A possible solution may be to add a small imaginary time component $t \rightarrow t-i\hbar\beta$, and to evaluate Eq.(3.23) via either newly developed stationary phase QMC methods 14,15 or via analytic continuation methods [16].

Now, I want to give a few indications of the type of results which can be generated with the present methods. In Figure 3.1, results for the vibrational relaxation of CO_2 in collisions with Pt(111) are shown. These were generated using the SST technique [9] including all energetically accessible ro-vibrational states in the basis, over 600 in all! The surface was smooth to eliminate the m_j and diffraction levels, but was movable in the z-direction to allow for energy exchange. The deexcitation probabilities are quite small, but very state specific. More efficient vibrational relaxation occurred for the significant fraction of trapped CO_2 molecules as compared to the scattered molecules shown in the Figure 3.1.

Next, in Figures 3.2 to 3.4, I show some results from experiments taken from a recent review by Rettner [17]. The original references, if available, are indicated on the figures. First, in Figure 3.1, the lack of rotational equilibration of NO at the surface temperature is shown. Figure 3.3 illustrates the detailed information on the rotational state of the scattered NO molecules as a function of kinetic energy, while Figure 3.4 shows the rather peaked and moderately wide angular distributions for two different final rotational levels. All the detailed features of these

(9a)

Surf Sci 176 (1986) 425

Table 1
Calculated vibrational energy levels for CO_2

Level index (ν)	State [a] ($\nu_1\nu_2^l\nu_3$)	Energy (eV)
1	00^00	0.0000
2	01^10	0.3145
3	02^00	0.3977
4	02^20	0.4716
5	10^00	0.4811
6	03^10	0.4892
7	03^30	0.5519
8	11^10	0.5659
9	00^01	0.5774
10	04^00	0.6036
11	04^20	0.6277
12	12^00	0.6349
13	04^40	0.6470
14	12^20	0.6499
15	20^00	0.6646
16	01^11	0.6703
17	05^10	0.6864
18	05^30	0.7074
19	13^10	0.7187
20	13^30	0.7347
21	21^10	0.7398
		0.7549

[a] Assignments above $\nu = 16$ may be unreliable because of the large mixture of harmonic basis functions used in the diagonalization of the CO_2 internal Hamiltonian.

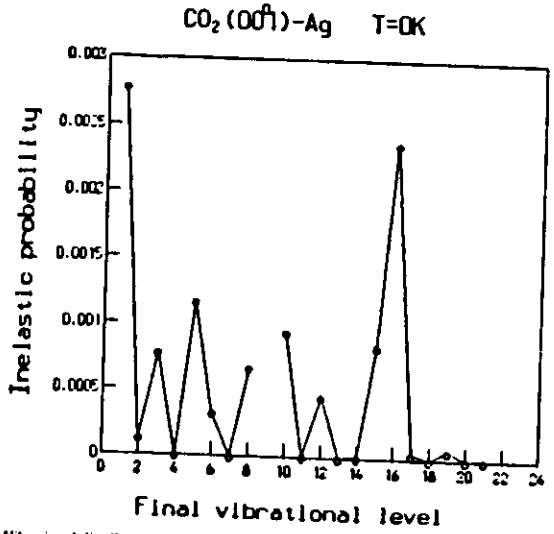

Fig. 5. Vibrational distribution for direct scattering of $CO_2(00^01) + Ag(111)$ at a kinetic energy of 0.125 eV at normal incidence. The surface temperature is 0 K. The (ν, J) basis was used as

Figure 3.1

(9b)

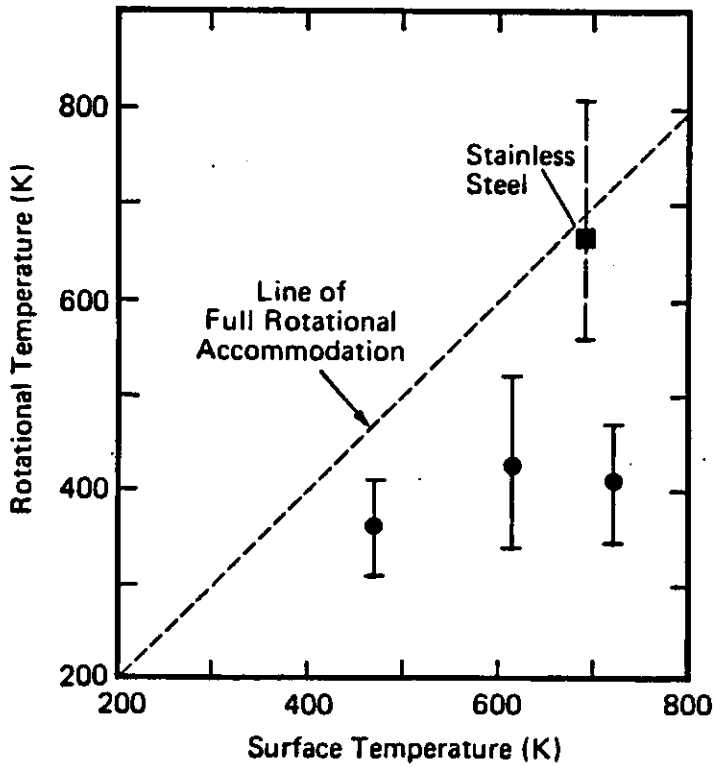

Figure 3.2

Figure 2. Rotational temperature of scattered NO molecules as a function of Ag(111) surface temperature (reference 3).

G.M McClelland, G.D. Kubiak, H.G. Rennagel and R.N. Zare,

(9c)

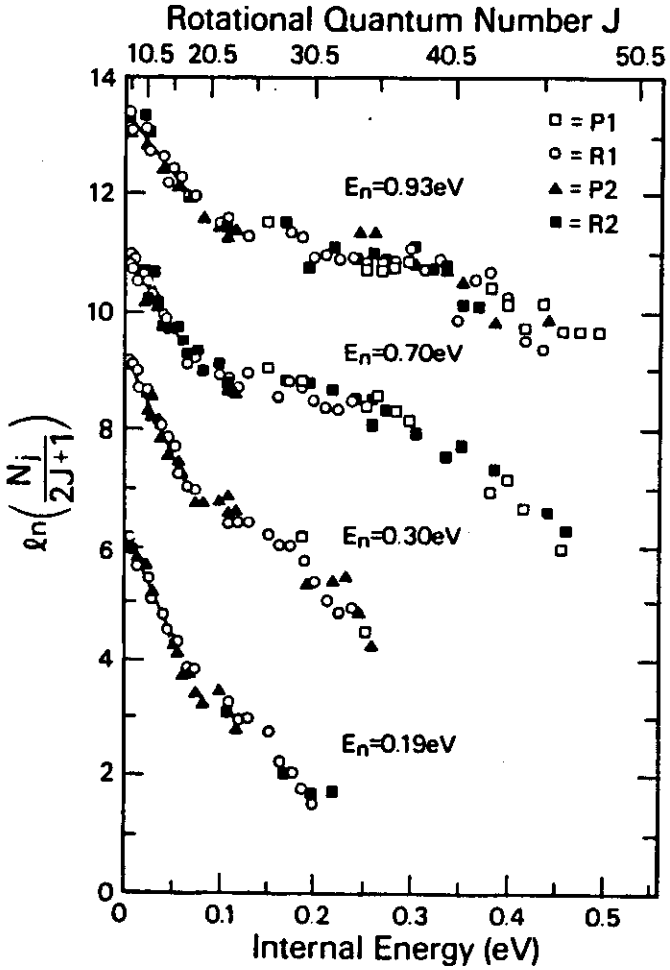

Figure 3.3

Figure 3. Rotational distributions obtained by Kleyn *et al.* (reference 4) for supersonic beams of NO scattering from Ag(111) with incident energies as indicated. The J scale applies to the $^2\Pi_{1/2}$ spin-orbit state.

A.W. Kleyn, A.C Luntz and D.J. Auerbach, Phys. Rev. Lett. 47 (1981) 1169; Surf. Sci 117 (1982) 33.

(9d)

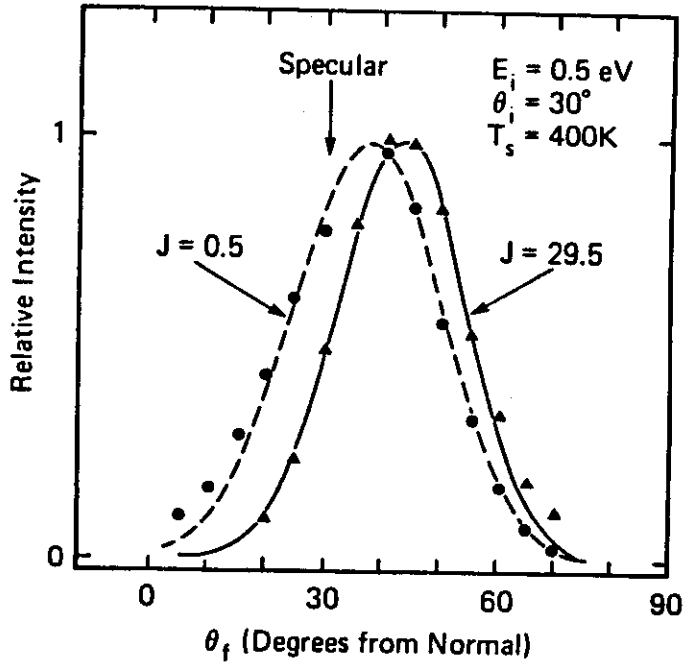

Figure 3.4

Figure 5. Angular distributions for NO (v=0, J=0.5) and NO (v=0, J=29.5) scattered from Ag(111) for E_i=0.5 eV, θ_i=30°, and T_s=400 K.

C.T. Rettner (private communication)

distributions are duplicated by classical trajectory-GLE-"ghost" atom simulations [18].

REFERENCES

1. J. C. Tully, private communication.

2. R. B. Gerber, R. Kosloff and M. Berman, Computer Physics Reports 5 (1986) 59.

3. R. C. Mowrey and D. J. Kouri, J. Chem. Phys. 84 (1986) 6466.

4. R. B. Gerber, "Molecular Scattering from Surfaces: theoretical methods and results", Chemical Reviews (1988).

5. R. B. Gerber, V. Buch and M. A. Ratner, J. Chem. Phys. 77 (1982) 3022.

6. N. Makri and W. H. Miller, J. Chem. Phys. 87 (1987) 5781.

7. A. M. Richard and A. E. DePristo, Surf. Sci. 134 (1983) 338.

8. C. Y. Lee, R. F. Grote and A. E. DePristo, Surf. Sci. 145 (1984) 466.

9. A. E. DePristo and L. C. Geiger, Surf. Sci. 176 (1986) 425.

10. G. Drolshagen and E. J. Heller, J. Chem. Phys. 79 (1983) 2072.

11. G. Drolshagen, Comments At. Mol. Phys. 17 (1985) 47.

12. B. Jackson and H. Metiu, J. Chem. Phys. 84 (1986) 3535.

13. B. Jackson and H. Metiu, J. Chem. Phys. 85 (1986) 4130.

14. J. D. Doll, D. L. Freeman and M. J. Gillan, Chem. Phys. Lett. 143 (1988) 277.

15. N. Makri and W. H. Miller, Chem. Phys. Lett. 139 (1987) 10.

16. A. E. DePristo, K. Haug and H. Metiu, Phys. Rev. Lett. (submitted).

17. C. T. Rettner, "Scattering of NO from Ag(111): a model system for probing gas-surface inelastic collision dynamics", (preprint).

18. C. W. Muhlhausen, L. R. Williams and J. C. Tully, J. Chem. Phys. 83 (1985) 2594; a newer PES has now been developed which is much better in duplicating all the available data, J. C. Tully (private communication).

MOLECULE SURFACE SCATTERING: IV

In this lecture, I consider the description of the simplest type of chemical reaction involving a gas molecule and a solid surface, namely the dissociative chemisorption of a diatomic molecule: $AB(g) + M \rightarrow A(a) + B(a) + M$. I will limit the treatment to the case when the surface is clean. The dissociation probability of a molecule upon collision with a clean surface is referred to as the zero-coverage sticking coefficient, S_o.

First I should mention that it is now possible to measure S_o by molecular beam scattering techniques [1-11] as a function of the molecule's incident kinetic energy, E_i, and direction as determined by the angle from the surface normal, θ_i. In addition the initial azimuthal angle can be fixed by orienting the crystal with respect to the incoming molecular beam. It is even feasible to excite a distribution of rotational and vibrational states of the incoming molecule. For most of the systems studied so far, S_o is found to be a function of the "normal" kinetic energy, $S_o(E_i,\theta_i,\phi_i)=S_o(E_i\cos^2\theta_i,0,\phi_i)$ but for a few systems it is found that S_o is a function of only the total kinetic energy, $S_o(E_i,\theta_i,\phi_i)=S_o(E_i,0,\phi_i)$. What is surprising about these findings is their simplicity, since in general one would not expect the combined effect of two variables to be represented so succinctly. Indeed, there are data which show neither type of scaling behavior. (Henceforth, I will suppress the explicit dependence upon ϕ_i for notational simplicity.) The explanation of such behavior is one goal of theoretical treatments of the dynamics. Another is to understand how factors such as the structure of the solid surface and the velocity and internal rotational-vibrational-electronic energy of the gas molecule influence the dissociation of the molecule on the surface. From a

practical view, I should mention that with this knowledge it may be possible to indicate how such reactions can be made more efficient and selective via modification of either the surface or the gas molecule.

It is feasible to perform realistic simulations of <u>reaction</u> dynamics in molecule-solid surface systems under zero coverage conditions [12-17]. These utilize the stochastic trajectory, GLE - "ghost" atom, techniques developed in lecture II to treat surface atom motion. The motion of the atoms in the gas molecule are also treated classically, by numerical integration of the Newtonian equations of motion. The particular system which results for a diatomic molecule-surface collision is:

$$m_1 d^2X_1/dt^2 = -\nabla_{X_1} V(\underline{X},\underline{Y},\{\underline{r}_\beta^o\}) \qquad (4.1a)$$

$$m_2 d^2X_1/dt^2 = -\nabla_{X_2} V(\underline{X},\underline{Y},\{\underline{r}_\beta^o\}) \qquad (4.1b)$$

$$d^2\underline{Y}/dt^2 = -\nabla_{\underline{Y}} V(\underline{X},\underline{Y},\{\underline{r}_\beta^o\}) - \underline{\Omega}^2 \underline{PP}\underline{Y} + \underline{M}_o^{\frac{1}{2}}\underline{\nu}_o\underline{s} \qquad (4.2)$$

$$d^2\underline{s}/dt^2 = \underline{\nu}_o\underline{M}_o^{\frac{1}{2}}\underline{Y} - \underline{\nu}_o^2\underline{s} - \underline{\tau}d\underline{s}/dt + \underline{f}(t) \qquad (4.3)$$

where $\underline{X}=(X_1,X_2)$ is the set of three dimensional positions for the two atoms of the diatomic. The most crucial feature controlling the accuracy of such simulations is the adequacy of the PES, which must be able to describe the breaking of the molecular bond and the making of two new atom-surface bonds. I will have much to say about such a PES later, but for now will simply assume that such a PES is available and focus on the mechanics of such a calculation.

For a particular initial kinetic energy (E_i) and angles (θ_i,ϕ_i) of the center-of-mass (CM) of the impinging molecule, one equation constrains $\underline{X}$,

$$m_1 d\underline{X}_1/dt + m_2 d\underline{X}_2/dt = (m_1+m_2)d\underline{X}/dt = M d\underline{X}/dt \qquad (4.4)$$

where the CM velocity components are specified. The initial z-component of $\underline{X}$ is restricted to be large in order to specify a free molecule plus

surface system initially. The in-plane components of the position $\underline{X}$ are constrained by the perfect 2D periodicity of the surface to lie within a given unit cell. And if the unit cell displays rotational symmetry then these are constrained to sample only the irreducible part of the unit cell. In any case, the two in-plane components of $\underline{X}$ are only specified to within some part of the unit cell. If the initial molecular vibrational (ϵ_n) and rotational (ϵ_J) energies are also specified, then we have

$$\tfrac{1}{2}\mu|dr/dt|^2 + v(r) = \epsilon_n \qquad (4.5)$$

$$\tfrac{1}{2}\mu r^{-2}|\underline{r} \times d\underline{r}/dt|^2 = \epsilon_J \qquad (4.6)$$

where $\underline{r}=\underline{X}_1-\underline{X}_2$ is the relative position vector, $v(r)$ is the interaction potential between the gas atoms in the absence of the surface (i.e. $V(\underline{X},\underline{Y},(\underline{r}\beta^o))$ as $|\underline{X}|\to\infty$), and μ is the reduced mass m_1m_2/M. Eq.(4.5) restricts the simultaneous variation of r and dr/dt, leaving one free. If I switch to action-angle variables, then the vibrational action is completely specified, while the angle is random. In other words, the vibrational phase can be chosen arbitrarily and still have the energy constraint in Eq.(4.5) be satisfied. Eq.(4.6) specifies only the magnitude of the rotational angular momentum vector. the orientation is free to be chosen. Thus, there are two angular variables left free. In combination with the freedom in the vibrational phase, there are three unspecified variables even by a completely energy selected initial condition. If the rotational polarization, with respect to some space-fixed Z-axis, of the initial rotational angular momentum was also chosen, then one less angular variable would be free. Such precise experiments may soon be feasible, but for now, one has three unspecified dynamical variables.

The net result of the above analysis is that 5 initial molecular

variables are not specified exactly, but are only restricted to be sampled from some distribution at the beginning of each trajectory. In addition, for a non-zero surface temperature, the initial velocities and positions of the primary and ghost atoms must be sampled. This can be done efficiently by finding the normal modes of the $(\underline{X},\underline{x})$ system and then sampling the velocities and positions from gaussian random distributions. For a typical primary zone of 13 atoms, there are 78 velocities and 78 positions to be sampled. The total number of variables to be sample is thus 161. Physically meaningful results for S_o are an average over all these variables of the form:

$$S_o = \int S_o(Q)P(Q)\,dQ \qquad (4.7)$$

where Q symbolizes all 161 random variables and $P(Q)$ is the relevant distribution function. Such an average is accomplished by the Monte-Carlo method with the number of Monte-Carlo points (i.e. trajectories) reflecting the desired accuracy of the quantity to be computed. However, a few hundred trajectories are typically needed even for large values of S_o=.5. If a less global quantity, such as the final angular-internal-kinetic energy distribution of the scattered molecules, is desired, then many more trajectories must be computed to provide statistically meaningful results.

I will discuss the results of various dynamical calculations later but now want to move on to a consideration of the PES in considerable detail. Let's focus on the basic physics of the interaction as described in a simple but very concise and useful model due to Norskov and co-workers [18]. At far distances from the surface, the molecule-surface interaction is a van der Waal's attraction, proportional to Z^{-3}. This is of little interest for a reactive PES since the electronic structure of the molecule

is unchanged. However, at closer distances, the affinity level (lowest unoccupied molecular orbital, LUMO) of the molecule begins to feel an image-charge type attraction, causing a shifting of its energy as

$$E_a(Z) = E_a(\infty) - 1/4Z \qquad (4.8)$$

As the distance Z gets smaller, the affinity level eventually gets pulled below the Fermi level of the solid, and the affinity level fills. If this level is anti-bonding, then the molecular bond may be weakened sufficiently to rupture, thereby effecting dissociative chemisorption. There is another process which competes with the lowering of the affinity level, namely the extra kinetic energy repulsion due to the Pauli exclusion principle operating between the solid's and molecule's electrons. If the latter increases more quickly than E_a decreases, a kinetic barrier to dissociation results. Indeed, if the breakdown in the image charge approximation occurs before the barrier is reached, the barrier may increase continually thereby leading to stable molecular physi- or chemi-sorption.

The above concepts indicate that electron transfer is a major cause of bond rupture at surfaces. With this in mind, Gadzuk and Holloway [19] have described the PES as the lowest eigenvalue of two diabatic curves, corresponding to the arrangements AB + S and AB^- + S^+. This quantifies the above ideas somewhat. However, the possible basic feature of a PES in any description of dissociative chemisorption are simple: 1/ a weak molecularly physisorbed species at far distances (4-8 bohr) from the surface; 2/ a barrier to the continued decrease in Z, separating a molecularly chemisorbed species; 3/ a barrier to stretching of the molecular bond, separating the final atomic chemisorbed products. A schematic diagram of such a PES is shown in Figure 4.1.

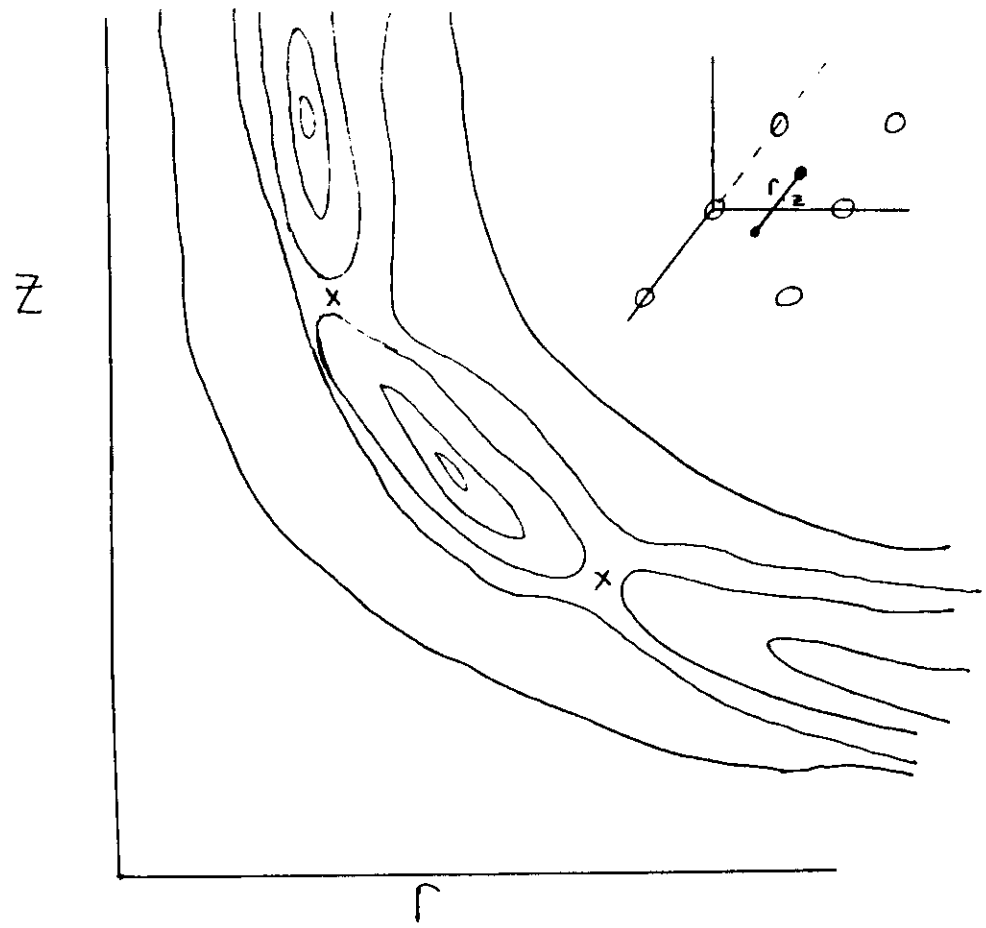

Figure 4.1

The main difficulty with such a simple argument is the neglect of the dynamics of the other degrees of freedom. The molecule can rotate and translate parallel to the surface, and the surface atoms can move, thereby distorting the PES. When the molecule rotates, the various barriers and even the gross topology of the PES changes. Similarly, the PES at different locations in the surface unit cell will be different. The dynamics in these other degrees of freedom may play a central role, and thus one must include them. This means that we must construct a full multi-dimensional PES to describe the reactive process.

It is worthwhile to emphasize that first principle or ab-initio calculations of full PES for dissociative chemisorption are not feasible with present day computers, given the accuracy (1-2 Kcal/mole, 0.05-0.1 eV) required by dynamical calculations. One must resort to a global representation with adjustable parameters at this time. While this leads to problems of uniqueness of the PES which I will address later, it does not lessen the importance of investigations of the dynamics since a quite general purpose is to provide insight into correlations between the topology of the PES and experimental data. However, there are now becoming available high quality calculations of at least a few points on the full PES and these can be used to fix some of the parameters in a representation of the full PES [20]. And these points can be extremely useful in determining the general topology of the PES. In particular, I should mention the results of Siegbahn et. al. on $H_2/Ni(100)$ modeled by an H_2/Ni_{38} cluster; these are ab-initio calculations using effective core potentials for the Ni electrons, but with a sophisticated ECP that can describe the response of the 3d electrons to changes in the 4s. These calculations have

been instrumental in determining a more optimal $H_2/Ni(100)$ PES [22] compared to the purely semi-empirical determination presented several years ago [12-14].

Let me now turn to one successful method of attack on this problem, initially developed by McCreery and Wolken [20] in the mid-1970's and later modified and quantified by Lee, Kara and DePristo [12,16]. The representation of the PES which has been used in a number of PES is a modified four-body LEPS form. Consider a diatomic, AB, interacting with a surface,S. The basic idea is to utilize the atom-surface interactions, V_{AS} and V_{BS}, and atom-atom interaction, V_{AB}, to construct the full molecule-surface interaction, $V_{AB,S}$ (which is the PES that I have been talking about throughout the lectures but just with more explicit notation here). The LEPS form is based upon use of a single valence electron for each body in the system. In a 3 body system, this allows only one bond. However, since the solid can bind both atoms simultaneously, two valence electrons are associated with the solid. The use of two electrons for the solid body is convenient mathematically, but this must not lead to a bond between these two electrons since this is nonsensical physically. Thus, the original four-body LEPS form must be modified to eliminate any non-physical electron-electron interactions. The rule is that each electron can only interact with an electron on a different body. This leads to the modified four-body LEPS form. Alternatively, one may consider this as a parametrized form with few parameters which have well controlled effects on the global PES.

The explicit form is,

$$V_{AB,S} = Q_{AS} + Q_{BS} + Q_{AB} - [J_{AB}(J_{AB}-J_{AS}-J_{BS})+(J_{AS}+J_{BS})^2]^{1/2} \qquad (4.9)$$

where Q and J are coulomb and exchange integrals, respectively, for each constituent. The central feature of this form is the non-additivity of the interaction potentials, which are Q+J for each body-body interaction. It is the precise division into Q and J that will control the activation barriers in the reaction. An inkling of this can be seen by noting that if the terms with A-S and B-S vanish, then $V_{AB,S}=Q_{AB}+J_{AB}=V_{AB}$. And,if the terms with A-B vanish, then $V_{AB,S}=(Q_{AS}+J_{AS})+(Q_{BS}+J_{BS})$. This will become clearer later, but first bear with me through the details of each type of term in Eq.(4.9).

First, consider the A-B interaction, since this is the simplest one given by:

$$Q_{AB} + J_{AB} = V_{AB}$$
$$= D_{AB}\,(\exp[-2\alpha_{AB}(r-R_{AB})] - 2\exp[-\alpha_{AB}(r-R_{AB})]) \qquad (4.10a)$$
$$Q_{AB} - J_{AB} = \tfrac{1}{2}[(1-\Delta_{AB})/(1+\Delta_{AB})]$$
$$D_{AB}\,(\exp[-2\alpha_{AB}(r-R_{AB})] + 2\exp[-\alpha_{AB}(r-R_{AB})]) \qquad (4.10b)$$

The A-B interaction potential is represented by the Morse potential in Eq.(4.10a). The parameters D_{AB}, α_{AB} and R_{AB} are the bond energy, range parameter and bond length, respectively, for the A-B molecule. These are specified by the A-B binding curve [23]. The A-B "anti-bonding" potential in Eq.(4.10b) is termed an anti-Morse form. The Sato parameter, Δ_{AB}, is unspecified as yet. However, it clearly controls the division of the Morse-anti-Morse forms into Q_{AB} and J_{AB}.

Now consider the A-S interaction. This is more complicated, given by:

$$Q_{AS} + J_{AS} = V_{AS}$$
$$= D_{AH}\,(\exp[-2\alpha_{AH}(r_{As}-R_{AH})] - 2\exp[-\alpha_{AH}(r_{As}-R_{AH})])$$
$$+ \Sigma\, D_{AS}\,(\exp[-2\alpha_{AS}(R_{A\beta}-R_{AS})] - 2\exp[-\alpha_{AS}(R_{A\beta}-R_{AS})]) \qquad (4.11a)$$

$$Q_{AS} - J_{AS} = \tfrac{1}{2}[(1-\Delta_{AS})/(1+\Delta_{AS})]$$
$$D_{AH}\,(\exp[-2\alpha_{AH}(r_{As}-R_{AH})] + 2\exp[-\alpha_{AH}(r_{As}-R_{AH})])$$
$$+ \tfrac{1}{2}[(1-\Delta_{AS})/(1+\Delta_{AS})]$$
$$\Sigma\, D_{AS}\,(\exp[-2\alpha_{AS}(R_{A\beta}-R_{AS})] + 2\exp[-\alpha_{AS}(R_{A\beta}-R_{AS})]) \qquad (4.11b)$$

The summation extends over all of the atoms in the crystal including the moving primary atoms and the fixed other atoms. The A-S bonding and "anti-bonding" potential are of similar form to those in Eq.(4.10). The distance between the atom A and the solid atom β is given by

$$R_{A\beta} = |\underline{R}_A - \underline{r}_\beta| \qquad (4.12)$$

The many more terms in Eq.(4.11) require further explanation.

First consider the terms in D_{AH}, which represent the interaction between A and the valence electrons of the metal. This is modeled by the interaction of A with jellium of density provided by the metal's valence electrons at the position of A. The parameters are thus:

1/ D_{AH} = strength of the interaction between atom A and jellium;
2/ α_{AH} = range of the above interaction;
3/ $R_{AH} = (3/4\pi n_o)^{1/3}$ where n_o is the density at the minimum of the atom-jellium binding curve.

These are taken from the SCF-LD first principle calculations of Puska et. al. [24] on the embedding energy of an atom in jellium as a function of the density of the jellium. Their numbers are represented by a Morse-like form. (It is not strictly a Morse potential since density is the variable instead of distance.) The variable, r_{As}, depends upon the density at the position of A:

$$r_{As} = (3/4\pi n)^{1/3} \qquad (4.13a)$$
$$n = \Sigma\, n(R_{A\beta}) \qquad (4.13b)$$

where $n(R_{A\beta})$ is the atomic density of the solid atom β at the center of the gas atom A and again the summation extends over all of the solid's atoms.

Note that I have assumed that the density above the metal surface is well represented by the sum over the individual atomic densities. Since differentiation of the PES is needed, simple forms are used for the atomic densities for each shell, where only the outer or valence electrons need be considered. For example, in W, the $6s^2$ and $5d^4$ are used:

$$n(R_{A\beta}) = 2n_s(R_{A\beta}) + 4n_d(R_{A\beta}) \qquad (4.14a)$$

where

$$n_s(r) = s_1[r-s_2]^{s4}\exp(-s_3 r) \qquad (4.14b)$$

$$n_d(r) = d_1\exp(-s_2 r^{s3}) \qquad (4.14c)$$

where the various parameters (s_k), (d_k) are determined by fitting to known atomic densities.

Next consider the terms in D_{AS}, which represent the interaction between A and the localized electrons and nuclear charge of the metal. This is modeled by a two body interaction between A and each solid atom, β, which is represented by a Morse potential. The parameters are defined below:

1/ D_{AS} = strength of the localized two body interaction between atom A and the solid's atoms
2/ α_{AS} = range of the above interaction
3/ R_{AS} = position of the minimum of the two body interaction

These parameters must be determined from information on the atom-surface interaction potential which may come from either sufficient experimental or theoretical information, such as the binding energy, height and frequency for different sites of adsorption or the full binding curves above each site.

The Sato parameter for the A-S interaction is Δ_{AS}. The B-S terms are exactly of the same forms but with different parameters, of course.

Note that since z_β is related by mass-weighting to the primary zone

displacement coordinates, the potential is dependent upon $\underline{y}$ and hence gives rise to forces, and energy exchange, between the gas molecule and the surface primary zone atoms.

REFERENCES

1. M. Balooch, M. J. Cardillo, D. R. Miller and R. E. Stickney, Surf. Sci. 46 (1974) 358.

2. M. J. Cardillo, M. Balooch and R. E. Stickney, Surf. Sci. 50 (1975) 263.

3. H. J. Robota, W. Vielhaber, M. C. Liu, J. Segner and G. Ertl, Surf. Sci. 155 (1985) 101.

4. H. P. Steinruck, K. D. Rendulic and A. Winkler, Surf. Sci. 154 (1985) 99.

5. H. P. Steinruck, M. Luger, A. Winkler and K. D. Rendulic, Phys. Rev. B 32 (1985) 5032.

6. A. V. Hamza and R. J. Madix, J. Phys. Chem. 89 (1985) 5381.

7. H. E. Pfnur, C. T. Rettner, J. Lee, R. J. Madix and D. J. Auerbach, J. Chem. Phys. 85 (1986) 7452.

8. C. T. Rettner and H. Stein, J. Chem. Phys. 87 (1987) 770.

9. C. T. Rettner and H. Stein, Phys. Rev. Lett. 59 (1987) 2768.

10. M. B. Lee, Q. Y. Yang, S. L. Tang and S. T. Ceyer, J. Chem. Phys. 85 (1986) 1693.

11. M. P. D'Evelyn, A. V. Hamza, G. E. Gdowski and R. J. Madix, Surf. Sci. 167 (1986) 451.

12. C. Y. Lee and A. E. DePristo, J. Chem. Phys. 85 (1986) 4161.

13. C. Y. Lee and A. E. DePristo, J. Vac. Sci. Tech. A5 (1987) 485.

14. C. Y. Lee and A. E. DePristo, J. Chem. Phys. 87 (1987) 1401.

15. A. Kara and A. E. DePristo, J. Chem. Phys. 88 (1988) 2033.

16. A. Kara and A. E. DePristo, Surf. Sci. 193 (1988) 437.

17. A. Kara and A. E. DePristo, J. Chem. Phys. 88 (1988) 5240.

18. J. K. Norskov, A. Houmoller, P. Johansson and B. I. Lundqvist, Phys. Rev. Lett. 76 (1981) 257.

19. J. W. Gadzuk and S. Holloway, J. Chem. Phys. 84 (1986) 3502.

20. P. Siegbahn, private communication of $H_2/Ni(100)$.

21. J. H. McCreery and G. Wolken, Jr., J. Chem. Phys. 67 (1977) 2551.

22. A. Kara and A. E. DePristo, to be published.

23. K. P. Huber and G. Herzberg, Constants of Diatomic Molecules (Van Nostrand, 1979).

24. M. J. Puska, R. M. Nieminen and I. Manninen, Phys. Rev. B24 (1981) 3037.

MOLECULE SURFACE SCATTERING: V

In this last lecture, I continue, and hopefully finish, the description of the dissociative chemisorption of a diatomic molecule. All of the theoretical parts are in place to allow treatment of real systems. I will focus in particular on the N_2/W(110) system [1-4] and the H_2/Ni(100) system [5-12].

I consider the N_2/W(110) system first, spending considerable time on the construction of the PES along the lines detailed in ref.[1]. Since the molecule is homonuclear, the parameters for the A-B-N atoms are identical. I use the explicit subscripts for the relevant bodies, but note that the references use a simpler notation which is also followed in the figures: 1/ $\Delta_{NW}=\Delta_{GS}$; 2/ $\Delta_{NN}=\Delta_{GG}$; 3/ $D_{NW}=D_2$; 4/$\alpha_{NW}=\alpha_2$; 5/ $R_{NW}=R_2$.

Typical results of the embedding energy for an atom in jellium are shown in Figure 5.1 based upon SCF-LD calculations [13]. For the N-atom, I find the Morse-like parameters modeling the embedding energy to be, $(D_{AH},\alpha_{AH},R_{AH})$=(1.4 eV, 0.78938 bohr^{-1}, 3.7575 bohr) with the last number corresponding to n_o=.0045 bohr^{-3}. From the atomic Hartree-Fock calculations for the W-atom [14], I find the 6s and 5d electron densities per electron are accurately represented over the important distance range 2 bohr<r<10 bohr by the forms of Eq.(4.14b-c) with the numbers given below:

$$n_s(r) = 0.1398[r-1.6992]^{1.1043}\exp(-1.3967r) \qquad (5.1)$$

$$n_d(r) = 0.078513\exp(-0.76027r^{1.5282}) \qquad (5.2)$$

All numbers are in a.u. The homogeneous part of the N-W potential is now completely specified.

To determine the two-body part of the N-W potential, I use the theoretical potential [15] shown in Figure 5.2, which is clearly strongly

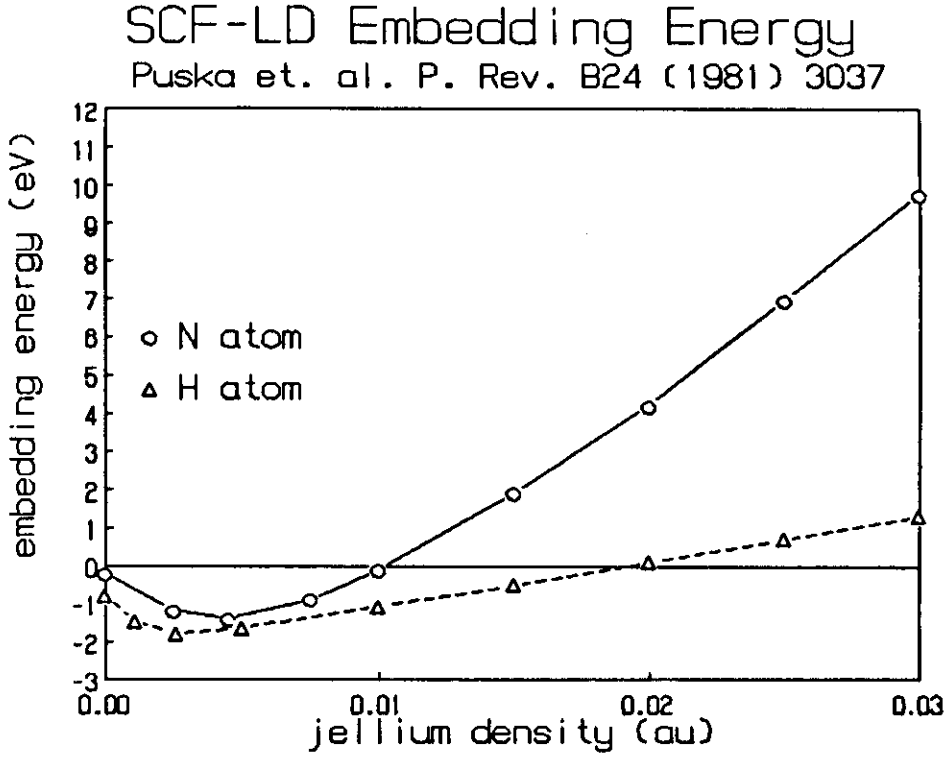

Figure 5.1

(11)

Surf Sci 193 (1988) 437

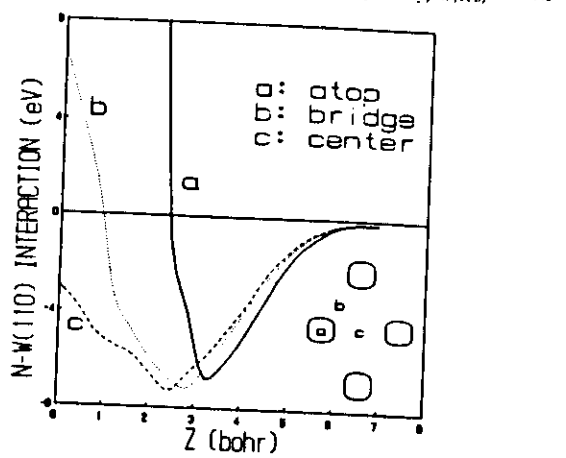

Fig. 1. Calculated N–W(110) interactions as a function of the height of the N above the surface for different sites. The CEM-1 method [25] was used.

Figure 5.2

dependent upon the binding site of the N-atom. The lowest minimum is in very good agreement with the experimental value of 6.73 eV [16]. Fitting Eq.(4.11) to the data in Figure 5.2 yields the remaining N-W potential parameters, $(D_{NW},\alpha_{NW},R_{NW})=(6.78\ eV,\ 1.089\ bohr^{-1},\ 2.354\ bohr)$. Note how large the two-body contribution to the N-W bond is compared to the homogeneous energy contribution, since the former has a minimum of -1.4 eV. Note also the small value of R_{NW} and the moderate value of α_{NW}, which combine to make the two body terms generally attractive (except close to the surface on an atop site) and relatively short-ranged. I should emphasize that the parameter values can change by a few percent and still provide an excellent fit to the theoretical potential in Figure 5.2. This will be important in providing flexibility in adjustment of the NN-W potential.

To complete all individual interaction potentials, I must specify $(D_{NN},\alpha_{NN},R_{NN})$. These are determined from the N_2 spectroscopic information [17] to be $(9.9\ eV,\ 1.42\ bohr^{-1},\ 2.06\ bohr)$.

Next, I want to illustrate the variety of topologies for the full NN-W interaction potential that can be generated by varying mainly the Sato parameters, Δ_{NW} and Δ_{NN}, and slightly the 2-body parameters, $(D_{NW},\alpha_{NW},R_{NW})$. I will show results for an N_2 molecule approaching a rigid W(110) surface with the N_2 molecular axis parallel to the surface, the center of mass above the bridge site and the two atoms pointing to opposite center sites, as illustrated in Figure 5.3. For the best PES, described later, this is the most favorable site and configuration for dissociation, and I will use it for the illustration. For each set of parameters a PES is calculated and a contour plot is made in the usual coordinates: bond length and

height. Since I cannot (and would not) show tens to hundreds of such plots to illustrate the parameter variation, I extract four critical features from each: the molecular well depth in the entrance channel; barrier energy; barrier location in both entrance channel (height) and exit channel (bond length). For the $N_2/W(110)$ system, this parameter variation did not ever yield two barriers since $(D_{NW}, \alpha_{NW}, R_{NW})$ were only allowed to vary slightly around the values specified above. (A different situation will exist for the $H_2/Ni(100)$ system discussed later). An entrance channel barrier is merely a convenient name for an activation barrier in which the molecular bond length is "nearly unchanged" from its gas phase value. By the same token, an exit channel barrier is one in which the molecular bond length is "significantly stretched" from its gas phase value.

First, consider the two Sato parameters which can vary from $-1<\Delta\leq 1$ in principle. I show results in Figure 5.3 for the range -0.8 to +0.8. All curves are shown for fixed Δ_{NW} as a function of Δ_{NN}. In the top panel, note that as either of the Sato parameters approaches -1, the barrier energy increases and the molecular well depth decreases. This is easy to understand since as either $\Delta \to -1$ the "anti-bonding" interaction increases to ∞ and it is the separation between the "bonding" and "anti-bonding" interaction which controls the size of the dissociation barrier. From the top panel of Figure 5.3, note two important points: 1/ for any reasonable sized barrier, there are an infinite set of Sato parameters; 2/ the molecular well depth can take on values from small ($\leq$0.1 eV) to large ($\geq$1.0 eV). Thus, the parametrized PES is quite flexible with regards to the relevant energies.

Next, consider the location of the barrier as shown in the middle and

Surf Sci 193 (1988) 437.

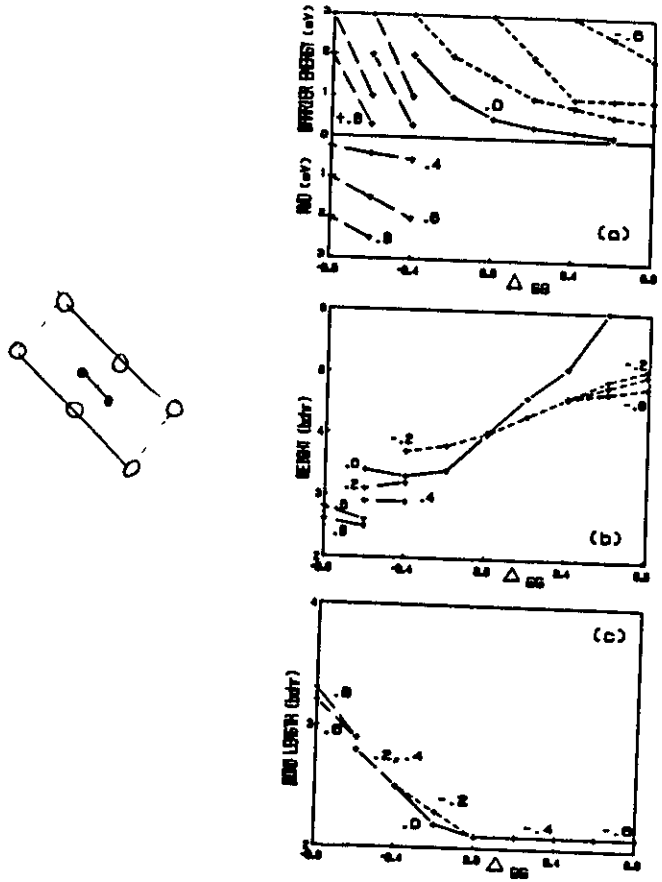

Fig. 3. (a) Activation barrier energy and molecular well depth (MWD) for the configuration in fig. 2 as a function of the N_2 Sato parameter. The different curves correspond to different values of the N–W Sato parameter as labeled on the figure. The symbols define the calculated points with the connecting line segments added for clarity; (b) same as (a) except for the height of the barrier above the surface; (c) same as (a) except for the bond length at the barrier location.

Figure 5.3

bottom panels of Figure 5.3. Some of the curves extend over a limited range because the barriers exist only over a small range. It is possible to place the barrier in either the entrance channel or the exit channel by variation of the Sato parameters.

To finish up this investigation of the variation of $V_{NN,W}$ with parameters, I show the effect of slight changes in the two-body parameters on the barrier height and molecular well depth in Figure 5.4. These changes have a very small effect on the location of the barrier, and thus this is not shown. By adjusting $(D_{NW},\alpha_{NW},R_{NW})$ it is possible to effect substantial change on the size of the activation barrier without varying the topology of the PES or the molecular well depth. This allows for a "fine tuning" of the PES.

I might emphasize that the original PES appears to lack sufficient flexibility but it is clear from a detailed analysis that this is not true. Indeed, there is such great flexibility that one might even wonder how these parameters can be fixed in any meaningful way. This can be accomplished because each parameter has a clear effect on the PES, which implies that certain types of experimental or theoretical information can greatly restrict the possible ranges. Let me address this problem in the context of the $N_2/W(110)$ system. For example, it is known [4] that the dissociation probability increases dramatically around E_i=0.5 eV, and I assume that this indicates some sort of barrier in the system; since there may be other effects, I simply use a reasonable range from 0-1 eV for such a barrier. From Fig. 5.3 one can see that this restricts Δ_{NW}>-0.4 but places no restrictions on Δ_{NN}. This information about the barrier energy alone does not reduce the range very much. It is also known [18] that the

(4a)

Surf Sci. 193 (1988) 437.

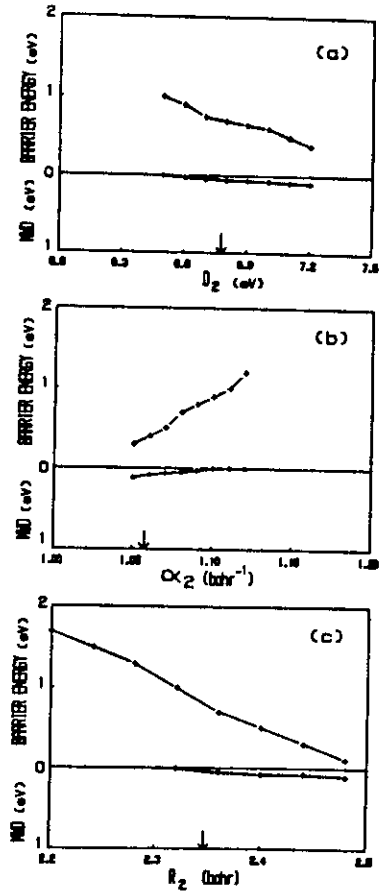

Fig. 4. (a) Same as fig. 3a except that the strength of the atom surface two body interaction, D_2, is being varied. The arrow indicates D_2 from table 1; (b) same as (a) except that the two body interaction range parameter, α_2, is being varied; (c) same as (a) except that the two body interaction minimum, R_2, is being varied. The Sato parameters are $\Delta_{GG} = -0.36$ and $\Delta_{GS} = 0.24$.

Figure 5.4

molecular well depth is ≈0.27 eV, and we use a reasonable range of 0-0.4 eV. This restricts $0.2<\Delta_{NW}<0.6$ and $-0.8\leq\Delta_{NN}\leq-0.2$. From both the barrier and well depth, the possible ranges are:

$$0.2\leq\Delta_{NW}\leq0.6 \qquad (5.3)$$

$$-0.4\leq\Delta_{NN}\leq-0.2 \qquad (5.4)$$

For these ranges, it is apparent from Figure 5.3 that the barrier lies in the exit channel (i.e. stretched N_2 bond length).

To determine the exact values of the Sato and two-body parameters, comparison is made between molecular beam scattering data and GLE-"ghost" atom stochastic trajectory results. This iterative process requires human intervention to adjust the parameters, and is best accomplished by use of supercomputers to minimize the "turnaround time". Of course, it is also greatly facilitated by intelligence in the choice of the parameters (e.g. by systematically carrying out the same type of investigation in Figures 5.3-4 for the system under study). The $N_2/W(110)$ provided an extremely difficult challenge because of the unusual experimental finding [4] that S_0 scales with the total kinetic energy, $S_0(E_i,\theta_i)=S_0(E_i,0)$. It was almost impossible to find a PES which gave such behavior. This can be understood by inspecting Figure 5.5a, which shows a cut through the final PES, and contrasting this with the PES in Figure 5.5b, which is representative of essentially all PES that did not give total kinetic energy scaling.

Focus on the PES in the bottom panel first which, after full multi-dimensional GLE-"ghost" atom simulations, yields S_0 shown in Figure 5.6. The results labeled 45N are generated assuming "normal" kinetic energy scaling, $S_0(E_i,45°)=S_0(E_i/2,0)$, and are in excellent agreement with those from the dynamical simulation at 45°. The surprising feature about such a

Surf. Sci. 193 (1988)

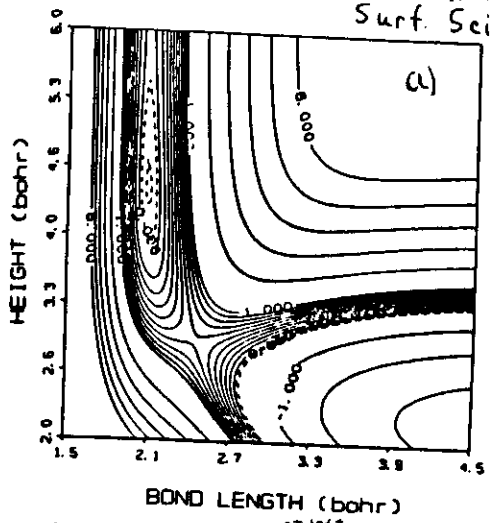

Fig. 7. Contour plot of the PES for the configuration shown at the top. The contour intervals are 0.1 eV up to 1.0 eV and 1.0 eV thereafter. The dashed curves are at −0.05 and −0.1 eV. The Sato parameters are $\Delta_{OO}=-0.369$, $\Delta_{OS}=0.241$, $D_3=6.81$ eV, $\alpha_3=1.05$ bohr^{-1}, $R_3=2.32$ bohr.

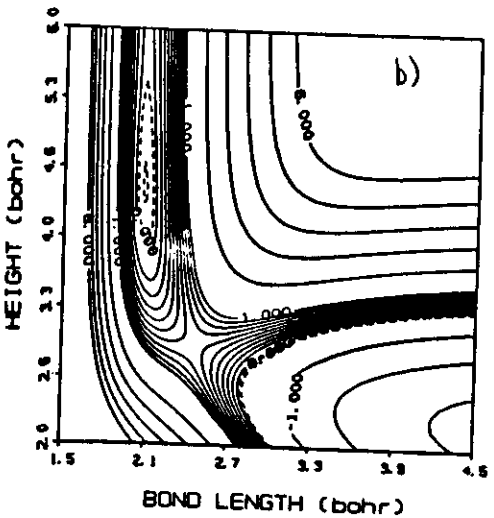

Fig. 8. Same as fig. 7 except for $\Delta_{OO}=-0.35$, $\Delta_{OS}=0.24$, $D_3=6.78$ eV, $\alpha_3=1.06$ bohr^{-1}, and $R_3=2.29$ bohr.

Figure 5.5

(5b)

Surf. Sci. 193 (1988) 437

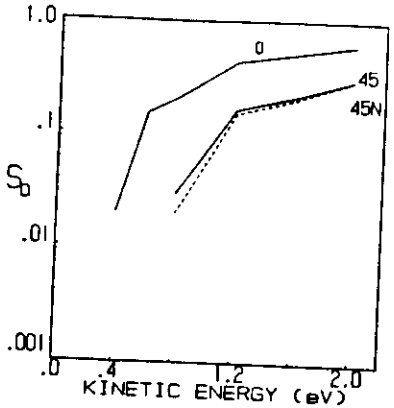

Fig. 9. Theoretical zero-coverage sticking coefficients for various initial kinetic energies and at two polar angles using the PES parameters from fig. 8. The value at 45N is generated from the normal kinetic energy scaling, $S_0(E, 45°) = S_0(E, \cos^2 45°, 0°)$.

Figure 5.6

"normal" kinetic energy scaling is that the PES in Figure 5.5b exhibits an exit channel barrier. This illustrates the danger in simply focusing on the location of the barrier and not considering the topology of the PES at least in the general region of the barrier. In Figure 5.5b, the shape of the PES slightly in the entrance channel around the barrier is such as to transform "normal" kinetic energy into vibrational energy. This makes an exit channel barrier act like an entrance channel one. I should conclude that observation of "normal" kinetic energy scaling is not particularly informative about the location of the PES barrier(s).

The distinguishing feature between the two PES in Figures 5.5a-b is the narrowness of the activation barrier region to motion perpendicular to the reaction path. The barrier region is extremely narrow in "a" but much flatter in "b". In other words, the PES in "a" enforces a much more stringent steric dependence on the molecule before reaction can occur. Although this PES also transforms "normal" kinetic energy into vibrational energy, such a process is too indiscriminate to enable just the correct bond length and height combination to surmount the low barrier. Instead, most trajectories lead to slightly wrong combinations of the height and bond length where the PES is much higher. Such a trajectory will not dissociate immediately but will transfer kinetic energy to the lattice phonons, molecular vibrations and rotations. If enough kinetic energy is transferred, the N_2 will not escape but will move out in height, move on the surface and then recollide with the surface, attempting another barrier crossing. Eventually, some trajectories will sample just the correct height, bond length (and site), and will still have enough energy to surmount the barrier. If we wait long enough, all will sample the lowest

barrier but not many will have enough energy to dissociate. In between, many of the N_2 molecules will transfer energy back to translations from rotations and vibrations, thereby desorbing. The question of the time scales for each of these processes can be addressed by the dynamical simulations, but has not been done so as yet. The results will depend upon the values of E_i, θ_i and the surface temperature, T_s.

It is clear, however, that the narrow barrier region makes the mechanism of the dissociation become rather indirect, thereby "scrambling" the translational velocity components, and leading to a total energy scaling as shown in Figure 5.7; the simulations show that the molecules often move 3-6 unit cells at E_i=1.2 eV before dissociating, but are <u>not equilibrated</u> with the surface and thus are not what would be described as classical precursors. It is interesting to note another consequence of the PES. In recombinative desorption, the nascent molecule will be formed at the activation barrier and then will move into the entrance channel region which transforms vibrational energy to translational energy. This will yield a desorption pattern that peaks around the normal to the surface. Thus, there is no contradiction between desorption intensities peaked around the normal and total energy scaling of S_0, at least in the N_2/W(110) system.

In the N_2/W(110) system, S_0 remains less than unity even at kinetic energies well above those of the minimum barrier shown in Figure 5.5a. This occurs because many initial configurations of the N_2 with respect to W(110) are repulsive and/or exhibit large activation barriers to dissociation and thus are scattered back into the gas phase. These molecules are also interesting to analyze, and this is done in Figures 5.8

(7a)

Surf Sci. 193 (1988) 437

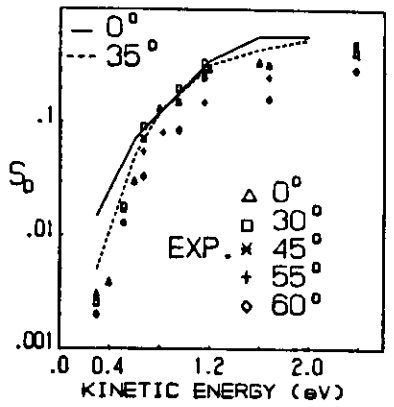

Fig. 5. Experimental and theoretical zero-coverage sticking coefficients for various initial kinetic energies and polar angles. The initial azimuthal direction is 0°.

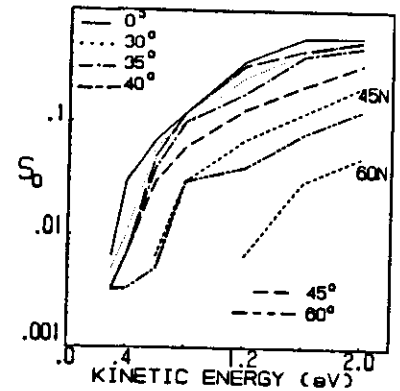

Fig. 6. Theoretical zero-coverage sticking coefficients for various initial kinetic energies and polar angles. The values at 45° and 60° generated from an assumed normal kinetic energy scaling, $S_0(E_i, \theta_i) = S_0(E_i \cos^2\theta_i, 0°)$, are labeled by 45N and 60N respectively.

Figure 5.7

(76)

Surf Sci. 193 (1988) 437

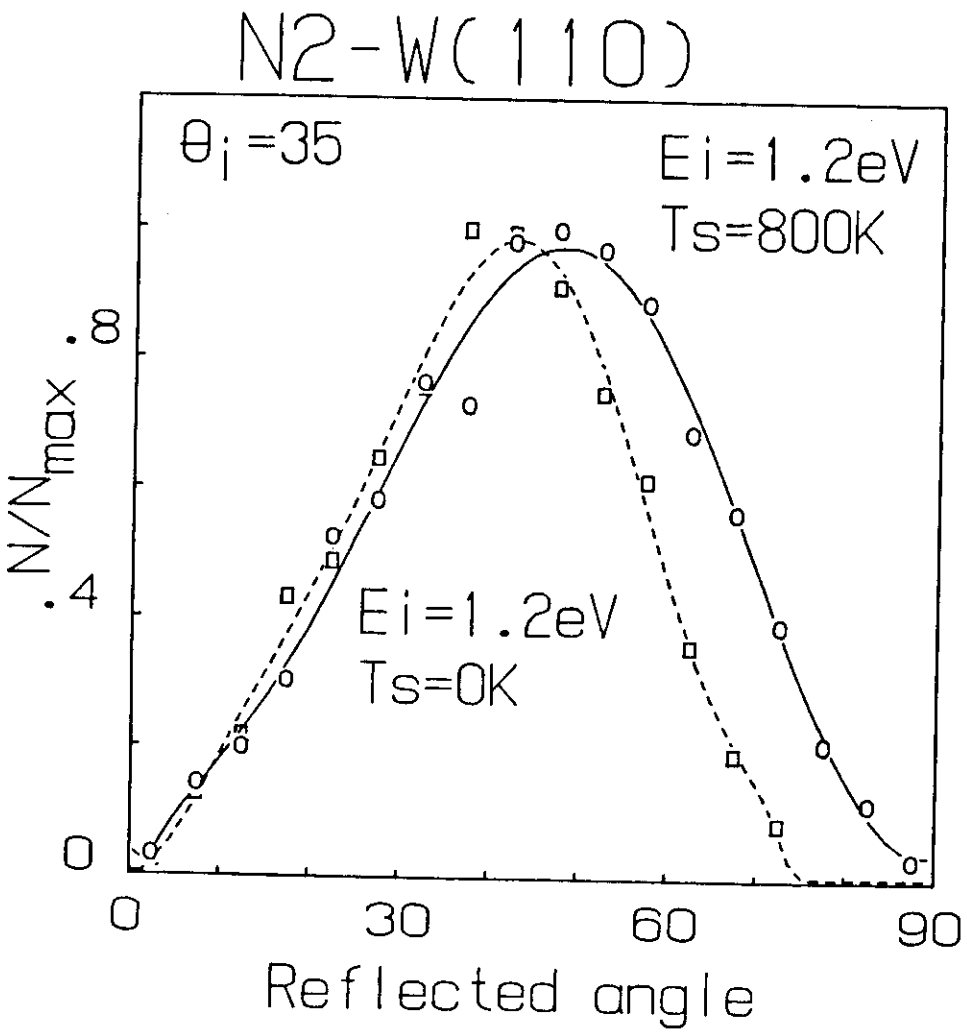

Figure 5.8

and 5.9 for the angular and energy distributions, respectively. The surprising feature of the angular distribution is its narrowness and peak at a slight supraspecular angle. The reason is that the molecules which scatter back into the gas-phase almost invariably only undergo a single impact with the surface, because of either an improper orientation or location during the initial collision. These scattered molecules do not sample the dissociative part of the PES but instead act just like the scattered molecules for inelastic scattering as described in lecture III. Further evidence for this is seen in Figure 5.9 which shows the distribution of rotational, vibrational, kinetic and total energy for all the scattered molecules, each summed over all final angles. The surprising result, which corroborates the above idea, is the negligible change in the vibrational energy even though E_i is high enough to excite $N_2(n=4)$. This demonstrates that the part of the PES which stretches the N_2 bond is not sampled by the scattered molecules. The scattering is not elastic however. The energy loss to W(110) is indicated by the average of the final TE being less than TE_i by about 0.3 eV. By contrast, the change in E_i is about 0.5 eV, which demonstrates that about 0.2 eV is transferred into rotations

Another interesting feature of the dissociative chemisorption is the dependence upon initial vibrational and rotational excitation of the N_2. The results in Figure 5.10 demonstrate that translational and vibrational energy are equally efficient at increasing S_o. This may be expected for a system in which total energy scaling is found, especially in light of the explanation for such scaling in terms of the PES in Figure 5.5a. By contrast, a complicated dependence upon rotational state is exhibited in

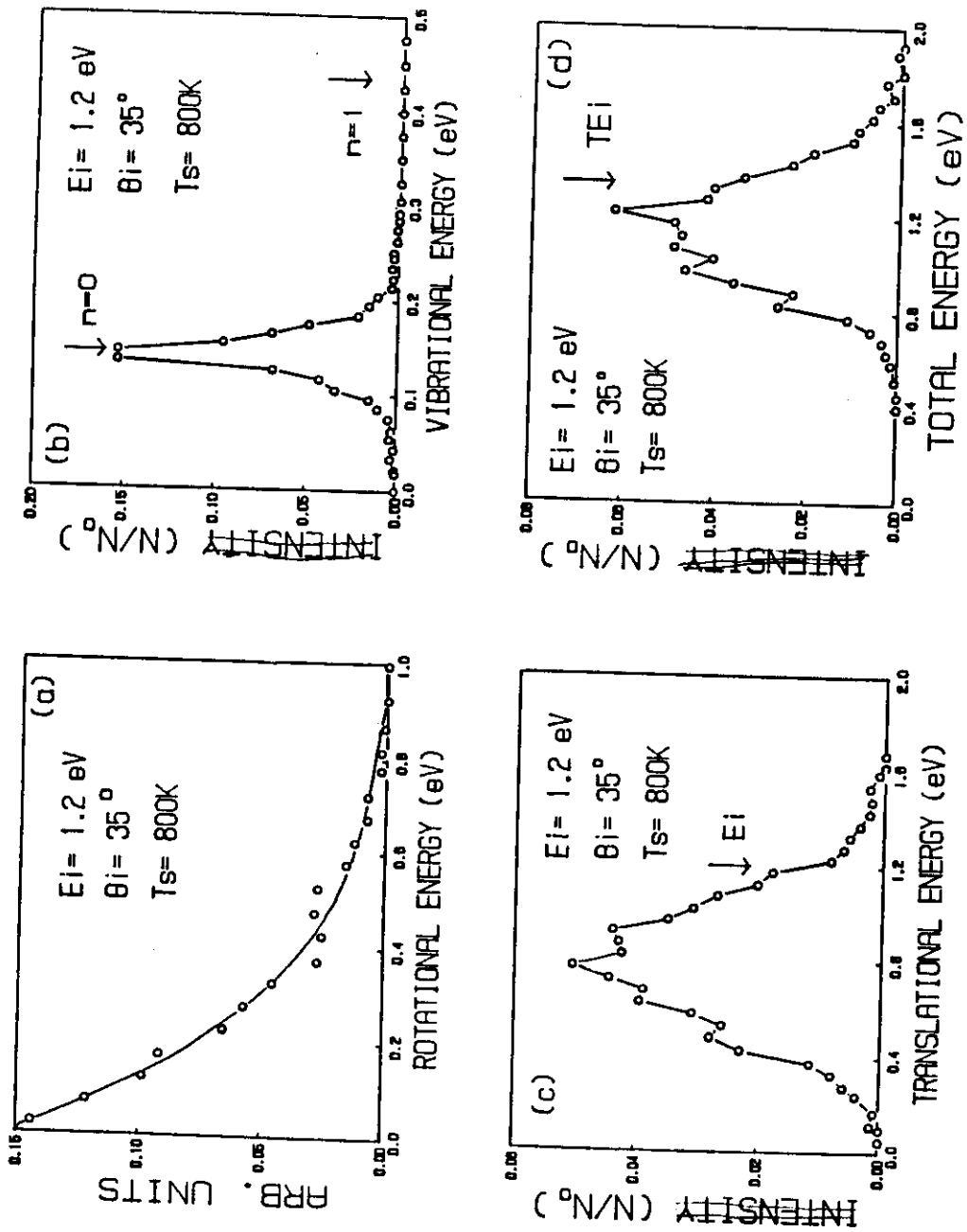

Figure 5.9

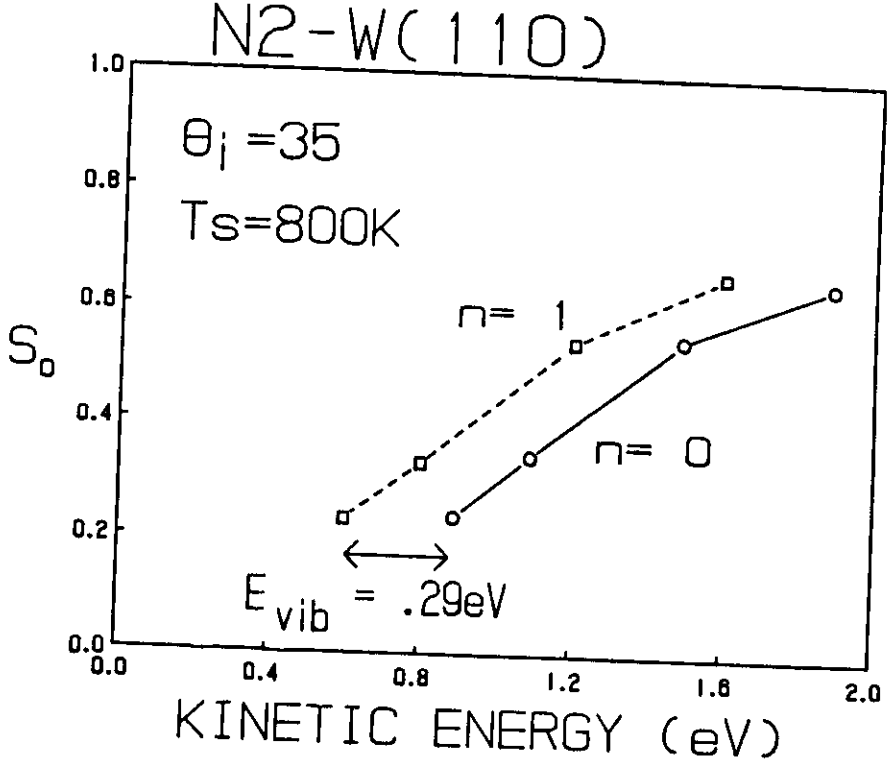

Figure 5.10

Figure 5.11. At each E_I there is a fast increase of S_o at j=2 followed by a nearly constant value. The increase is much larger than the variation of S_o with E_I since $\epsilon_{j=2} \approx .0015$ eV. The reason for the j-dependence can be seen in Figure 5.12 in terms of the variation of the dissociation probability with initial orientation of $\hat{j}$: larger dissociation occurs for $\hat{j}$ oriented parallel to the surface (i.e. rotating in the plane of the surface). This is due to both a geometric effect (i.e. rotations in the plane sample the dissociation barrier more fully) and a dynamical effect (i.e. small rotational energy perpendicular to the plane allows for significant translational to rotational energy transfer, increasing the surface residence time and thus S_o). It appears that the dependence of S_o on j is a complicated and quite informative piece of data.

I now want to turn to treatment of a different type of system, H_2 colliding with Ni and Cu surfaces. The light mass of H_2 precludes significant energy transfer to the lattice, and indicates that S_o should proceed by a direct mechanism if possible. However, since H_2 is so light it is important to identify possible quantum mechanical effects. For the dissociation of H_2 fixed parallel to the surface on a rigid linear chain of Ni atoms, spaced as along a row of Ni(100), the exact solution of the time-dependent Schrodinger equation is feasible as outline in Lecture I. This has been accomplished [10,11] using the FFT algorithm with the PES and dynamical results shown in Figure 5.13. The classical and quantum values of S_o are in general agreement except at the lowest kinetic energies. Even for H_2, the classical results are not terrible, but are clearly not quantitative. This is due to both quantum mechanical tunneling and reflection of the wavefunction at the second atop position as the H-atoms

J. Chem. Phys 88 (1988) 5640

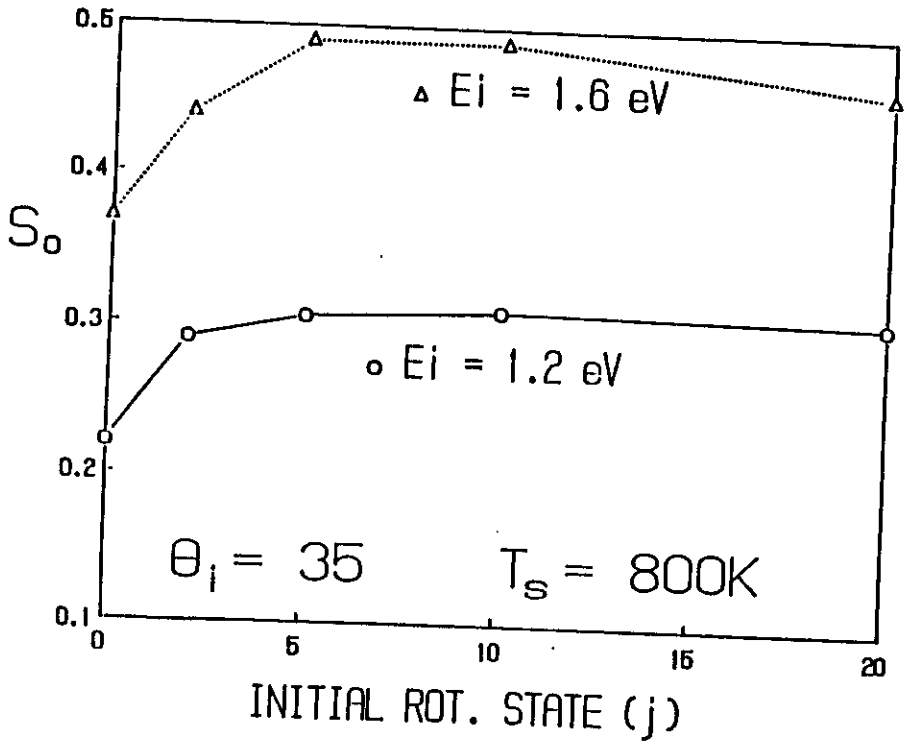

Figure 1. Variation of the dissociation probability with initial rotational state of the N_2 for two different initial kinetic energies.

Figure 5.11

J. Chem. Phys. 88 (1988) 5640 M. Cardillo and B. Jackson, J. Chem. Phys. 87 (1987) 4497.

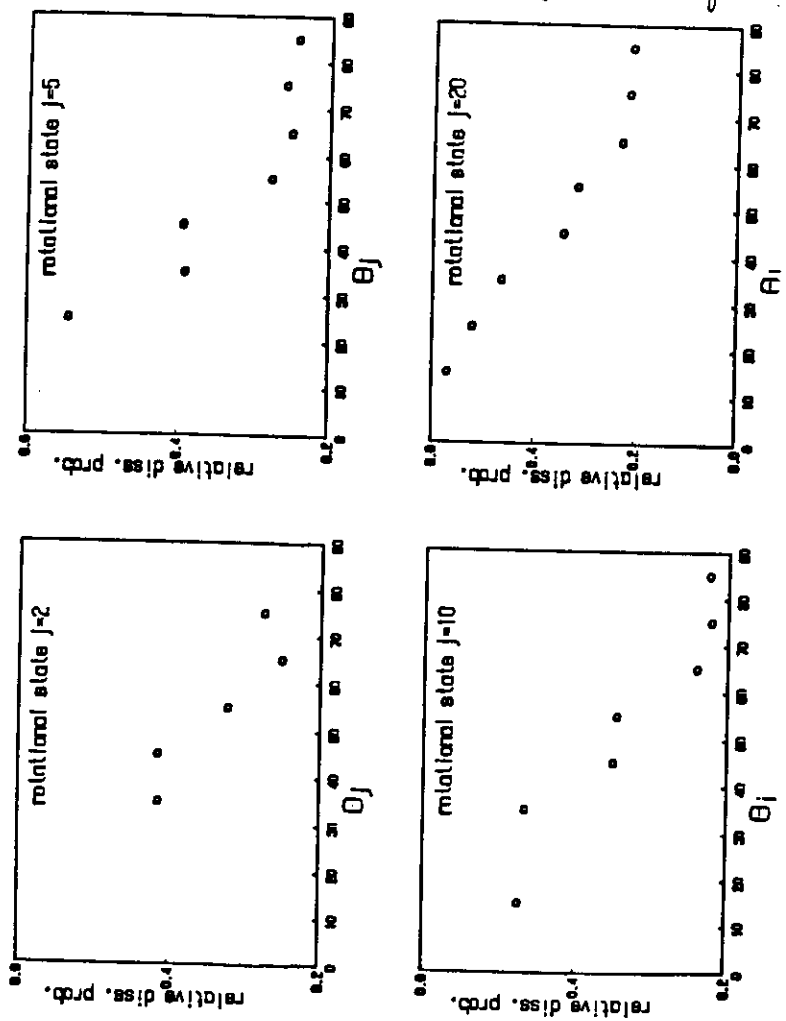

Figure 2. Variation of the relative dissociation probability (number of dissociating trajectories divided by the initial angular distribution) with initial orientation of the rotational angular momentum vector with respect to the surface normal. Angles near 0° correspond to a molecule rotating parallel to the plane of the surface.

Figure 5.12

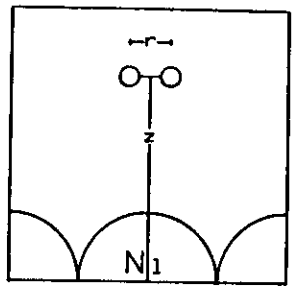

FIG. 1. Geometry and coordinate system used to study hydrogen dissociation on Ni(100). r is the full bond length and z is the distance of the molecule's center of mass above the plane of surface Ni atoms.

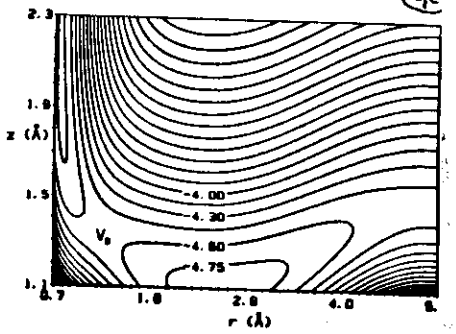

FIG. 2. LEPS potential surface for the atop-to-bridge site dissociative ... sorption of hydrogen on Ni(100). The energy contour spacing is 0.15 ... The parameters, listed in Table I, were chosen to reproduce the transiti... and bound state regions computed by Seoghaha *et al.* (Ref. 13). V_b deno... the barrier to dissociation.

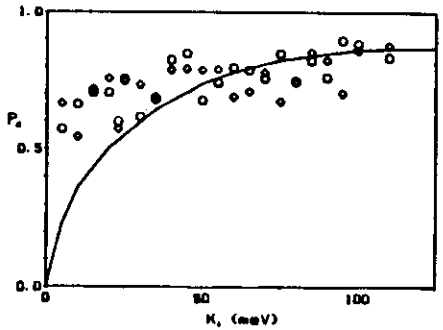

FIG. 3. The dissociative sticking probability P_d as a function of the initial molecular kinetic energy K_i, for H_2 on Ni(100). The solid curve is from the quantum calculation, and the circles and diamonds correspond to the quantum-weighted classical and quasiclassical approaches, respectively.

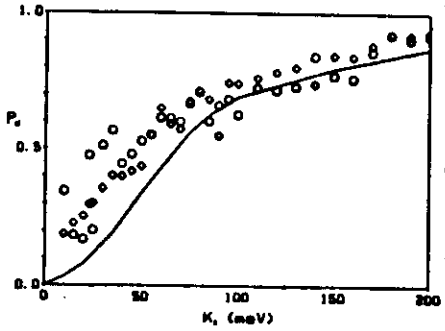

FIG. 4. Same as Fig. 3, except for D_2.

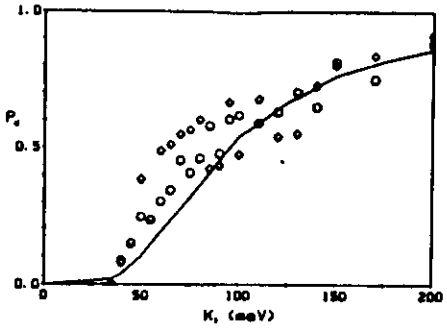

FIG. 5. Same as Fig. 3, except for T_2.

Figure 5.13

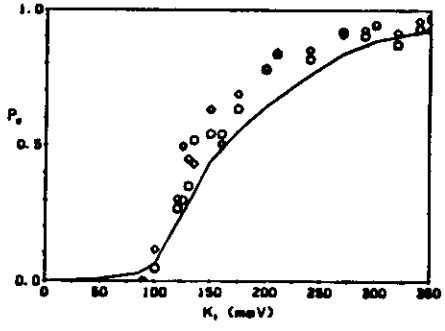

FIG. 6. Same as Fig. 3, except for an hypothetical hydrogen isotope with an atomic mass of 7 amu.

separate on the surface. The latter effect will be negligible on a real 3-D surface.

I should mention a different approach to investigation of reactive scattering of H_2 on Ni and Cu, due to Halstead and Holloway [19]. They assume an activation barrier in the entrance channel that varies for different positions of the H_2 in the surface unit cell but which is independent of the orientation and bond length of the H_2. Under these approximations, the dynamical equations become identical to those of an atom scattering from a rigid, corrugated surface, and thus one can treat diffraction, tunneling and dissociative chemisorption by accurate quantum techniques. In their paper, the equations are solved by the FFT procedure. The justification for the former approximation is the absence of rotational effects in the physisorbed species. The justification for the latter approximation is the absence of a stretched molecular bond at the position of the activation barrier(s). Further work will be need to ascertain whether such an assumptions are valid.

Finally, let me briefly consider a new PES for the H_2/Ni(100) system [8]. This is based upon recent ab-initio calculations of Siegbahn [12] along with dynamically adjusted Sato parameters. Contour plots in Figure 5.14 demonstrate that there are small activation barriers of ≈0.035 eV and ≈0.045 eV in the entrance channel of "a'" and "b'", respectively, but that at least for the atop->center dissociation, there is also a barrier in the exit channel. The orientation dependence of the entrance channel barrier has not been determined quantitatively yet, but the vibrational dependence is quite weak. And the variation with position in the unit cell is also weak. However, the exit channel barrier obviously has a strong dependence

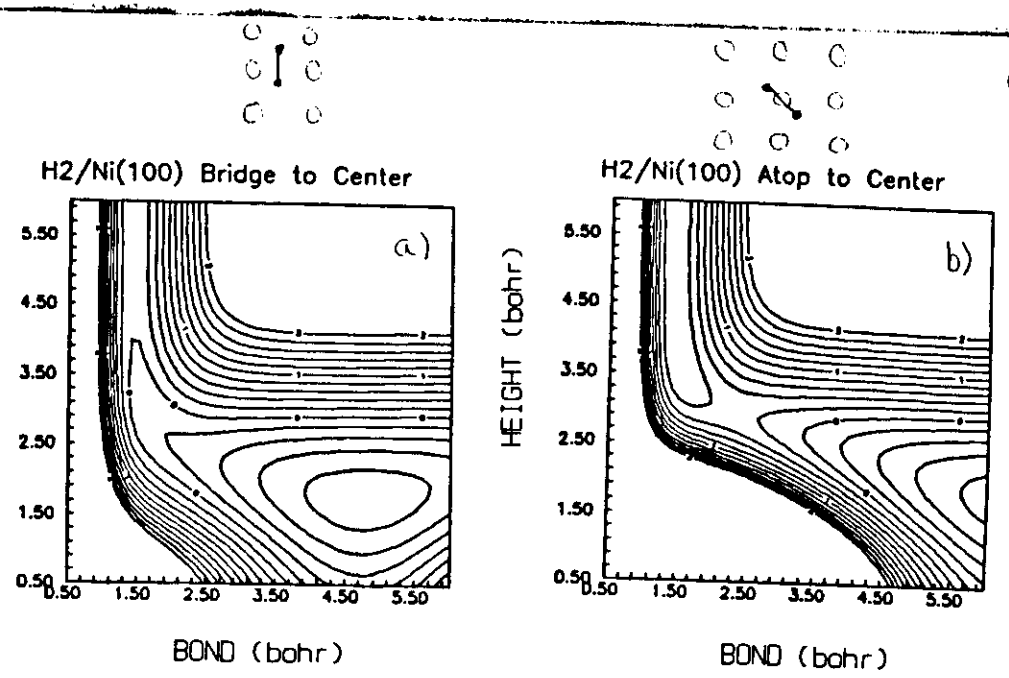

ZOOMING THE ENTRANCE CHANNEL

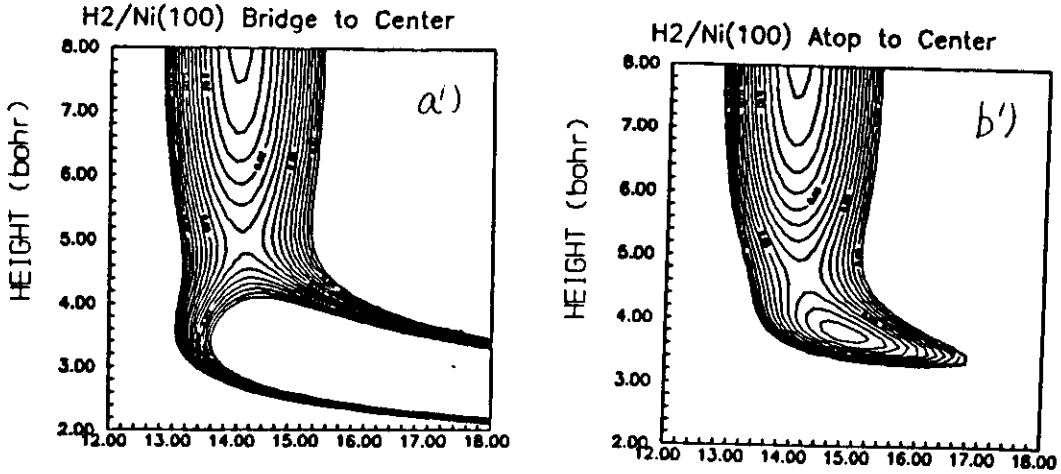

Figure 5.14

upon bond length. Thus, the PES is more complex than assumed in reference 19, but it is not apparent how the other features than the entrance channel barrier affect the dynamics.

To provide some understanding, we have performed classical simulations in which all degrees of freedom of H_2 can be included. The surface was allowed to move initially but this gave negligible effects, and all the results in Figure 5.15 are for a rigid surface. There must be some dynamical features of orientation and bond length since S_o in Figure 5.15 does not become unity at E_i>0.1 eV, which exceeds all the entrance channel barriers. On the other hand, $0.6 \leq S_o \leq 0.7$ at such energies and so most of the molecules do dissociate after surmounting the entrance channel barrier. And, the angular distribution of scattered molecules is quite narrow, indicating small translational to rotational energy transfer. Perhaps the most interesting illustration of the importance of rotations is the dependence of S_o on initial rotational state of the H_2. As for the N_2/W(110) system, the dependence is quite complex but it is clear from the decrease of S_o at high j that the dynamics after passage over the entrance channel barrier(s) must play a considerable role since by j=8, S_o decreases by 50% from the j=0 result.

Much more work is needed to understand the above behavior. Indeed, while much is known about the dynamics of a few simple molecule-surface reactions, very few general rules and little global understanding is available. At this stage, every system presents a new challenge and new characteristics. They also present new opportunities, and that is perhaps the best statement to remember.

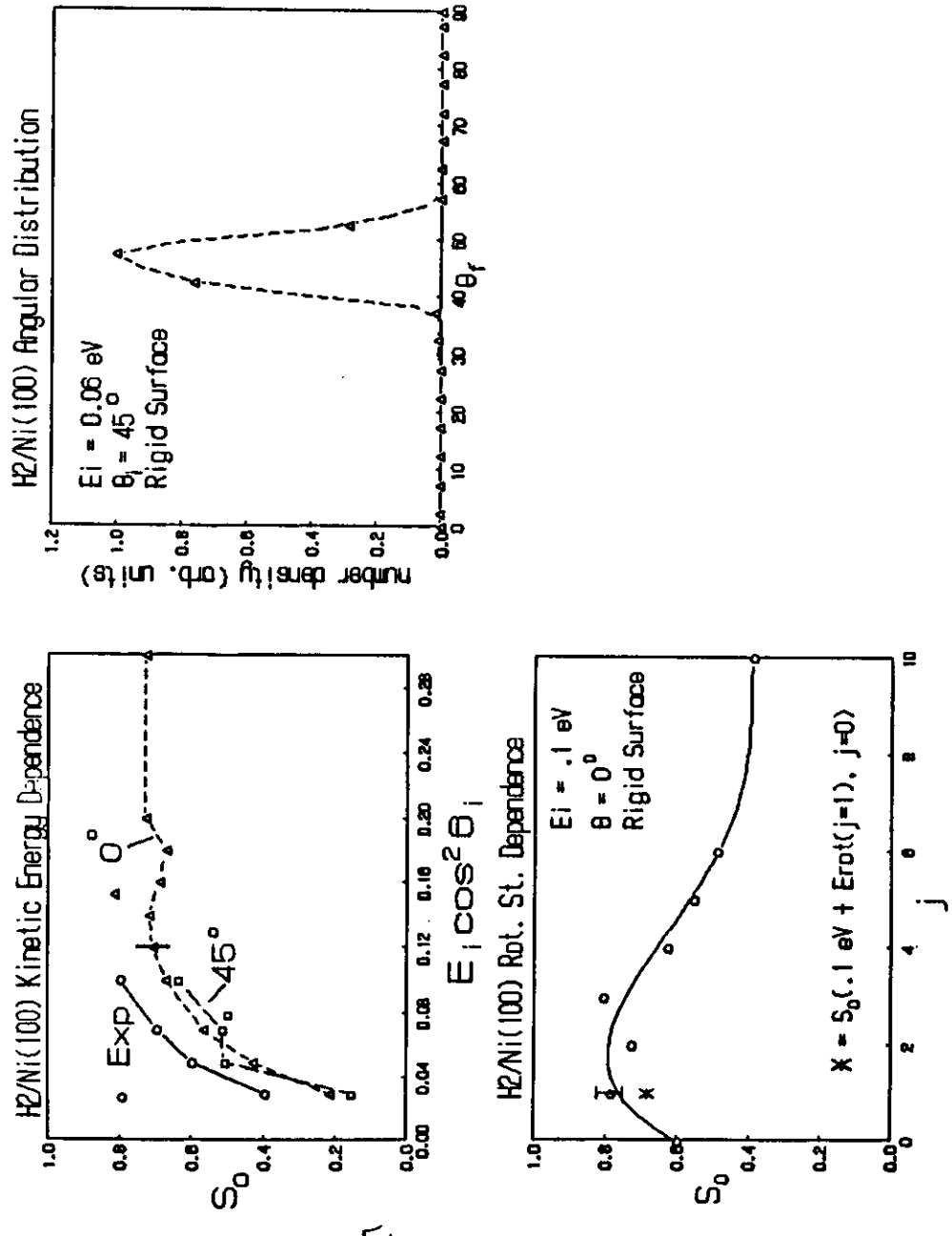

Figure 5.15

REFERENCES

1. A. Kara and A. E. DePristo, Surf. Sci. 193 (1988) 437.

2. A. Kara and A. E. DePristo, J. Chem. Phys. 88 (1988) 2033.

3. A. Kara and A. E. DePristo, J. Chem. Phys. 88 (1988) 5240.

4. H. E. Pfnur, C. T. Rettner, J. Lee, R. J. Madix and D. J. Auerbach, J. Chem. Phys. 85 (1986) 7452.

5. H. P. Steinruck, K. D. Rendulic and A. Winkler, Surf. Sci. 154 (1985) 99.

6. H. P. Steinruck, M. Luger, A. Winkler and K. D. Rendulic, Phys. Rev. B 32 (1985) 5032.

7. A. V. Hamza and R. J. Madix, J. Phys. Chem. 89 (1985) 5381.

8. A. Kara and A. E. DePristo, to be published.

9. C. Y. Lee and A. E. DePristo, J. Chem. Phys. 85 (1986) 4161; 87 (1987) 1401; J. Vac. Sci. Tech. A5 (1987) 485.

10. C. M. Chiang and B. Jackson, J. Chem. Phys. 87 (1987) 5497.

11. B. Jackson and H. Metiu, J. Chem. Phys. 86 (1987) 1026.

12. P. Siegbahn, private communication of H_2/Ni(100) ab-initio calculations PES.

13. M. J. Puska, R. M. Nieminen and I. Manninen, Phys. Rev. B24 (1981) 3037.

14. A. D. McLean and R. S. McLean, At. Data Nucl. Data Tables 26 (1981) 197.

15. These were computed by the method detailed in J. D. Kress and A. E. DePristo, J. Chem. Phys. 87 (1987) 4700.

16. W. Ho, R. F. Willis and E. W. Plummer, Surf. Sci.95 (1980) 171; P. W. Tamm and L. D. Schmidt, Surf. Sci. 26 (1971 286.

17. K. P. Huber and G. Herzberg, Constants of Diatomic Molecules (Van Nostrand, 1979).

18. J. T. Yates, R. Klein and T. E. Madey, Surf. Sci. 58 (1976) 469.

19. D. Halstead and S. Holloway, "Quantum Mechanical Scattering of H_2 from Metal Surfaces: diffraction and dissociative adsorption," J. Chem. Phys. (in press).

ACKNOWLEDGEMENT

This work has been supported over the past six years mainly by the National Science Foundation, division of Chemical Physics. Partial support by the Petroleum Research Foundation administered by the American Chemical Society has also been received. Generous amounts of supercomputer time, provided by NSF mainly at the Pittsburgh Supercomputer Center, made this research possible. Finally, much of the research on reactive scattering is the result of the cleverness, persistence and physical insight of Drs. Abdelkader Kara and Chyuan-Yih Lee. By the same token, the work on semiclassical inelastic scattering is mainly due to Drs. Ann M. Richard and Lynn C. Geiger.